



# **Constituent Quarks and the Gluonic Contribution to the Spin of the Nucleon**

**Ludwig-Maximilians-Universität München**  
**Faculty of Physics**

**Thesis submitted**  
**By**  
**Gamal Eldahoumi**  
**from Benghazi/Libya**

**Munich**  
**January 2009**

**First Supervisor: Prof. Dr. Harald Fritzs**

**Second Supervisor: Prof. Dr. Ivo Sachs**

**Date of examination: April 29, 2009**

## **ABSTRACT**

The internal structure of the nucleon is more complicated than expected in a simple quark model. In particular, the portion of the nucleon spin carried by the spins of the quarks is not, as expected, of the order of one, but according to the experimental data much smaller. In this thesis we study the spin structure of the proton in quantum chromodynamics.

The constituent quark model, based on  $SU(6)$ , predicts that the spin of the proton should be carried by the quarks, in disagreement with the experiments. It appears strange, that the theoretical model works so well for the magnetic moments of the nucleons, but not for the spin, although the spin and the magnetic moments are closely related to each other. We shall resolve this problem by assuming that the constituent quarks have an internal structure on their own. Thus a constituent quark has a dynamical structure, and we can introduce notions like the quark or gluon distributions inside a constituent quark.

In the light of new experimental data from HERMES, COMPASS, J-Lab, and RHIC-spin, the current status of our knowledge of the spin structure is discussed in the two theoretical frameworks: the naive parton model, and the QCD evolved parton model. QCD is a successful theory, both in perturbative and non-perturbative regions, but the spin of the nucleon still needs to be explained within QCD.

# CONTENTS

---

	<i>Page</i>
Abstract . . . . .	i
Introduction . . . . .	1
<b>1 The nucleon</b> . . . . .	<b>3</b>
1.1 What do we know about the nucleon? . . . . .	3
1.2 The substructure of the nucleon . . . . .	4
1.3 Experimental aspects . . . . .	8
1.3.1 Electromagnetic interaction . . . . .	8
1.3.2 The strong Interaction . . . . .	10
1.3.3 The weak interaction . . . . .	10
<b>2 Theoretical framework</b> . . . . .	<b>11</b>
2.1 The Gluon in the Nucleon and the Gluon Polarisation . .	11
2.2 Deep inelastic scattering . . . . .	11
2.2.1 The formalism of polarized deep inelastic scattering . . . . .	12
2.2.2 Theoretical models . . . . .	16
2.2.3 Sum rules in polarised deep inelastic scattering . .	17
2.3 Interpretation in the Quark Parton Model. . . . .	18
2.3.1 The distributions of Partons. . . . .	19
2.3.2 The Spin of the Nucleon and the first Moment of the spin-dependent structure function $g_1(x, Q^2)$ .	23
2.4 Improved Parton Model in QCD . . . . .	30
2.4.1 Scaling Violations . . . . .	30
2.4.2 QCD Evolution Equations . . . . .	32
2.4.3 The Axial Anomaly . . . . .	39
2.5 Fragmentation . . . . .	40

<b>3</b>	<b>Gluon Helicity Distribution <math>\Delta G(\mathbf{x}, Q^2)</math></b> .....	44
3.1	Next-to-Leading Order Evolution of $g_1(x, Q^2)$ .....	45
3.2	Gluon helicity distribution from the QCD Scale Evolution.....	50
3.3	Gluon helicity distribution from Di-jet Production in $e-p$ Scattering .....	52
3.4	Gluon helicity distribution from Large- $p_T$ Hadron Production in $e-p$ Scattering .....	55
3.5	Gluon helicity distribution from open-charm (heavy-quark) production in $e-p$ Scattering .....	56
3.6	The gluon helicity distribution from direct photon production in $p-p$ collisions .....	59
3.7	Gluon helicity distribution from jet and hadron production in $p-p$ collisions .....	62
<b>4</b>	<b>The Spin of the Proton</b> .....	64
4.1	Model of the proton spin structure .....	70
4.2	Phenomenology of the model .....	72
4.3	Experimental Measurements of the gluon distribution .	75
4.4	Constituent Quarks in QCD .....	78
	Summary and conclusion .....	87
	<b>Acknowledgment</b> .....	88
	<b>References</b> .....	89

---

## List of Figures

	<i>Page</i>
1.1 Scheme of a polarized electron-polarized proton scattering experiment. . . . .	5
1.2 Simplest quark model of the proton and neutron. . . . .	7
1.3 Simplest quark model of a polarized proton. . . . .	7
2.1 The basic diagram for deep inelastic lepton hadron scattering. . . . .	12
2.1 Distributions of $x$ times the unpolarised parton distributions $f(x)$ (where $f = u_v, d_v, \bar{u}, \bar{d}, s, c, g$ ) using the MRST2001 parametrisation [30,31] (with uncertainties for $u_v, d_v$ and $g$ ) at a scale of $10\text{GeV}^2$ . Figure taken from [32]. . . . .	22
2.3 Direct determination of the gluon distribution at HERA. The measured gluon density at an average $Q^2$ of $30\text{GeV}^2$ is compared with the indirect determinations by H1 [33] and ZEUS [34] at $Q^2 = 20\text{GeV}^2$ , and with a determination from $J/\Psi$ production by NMC [35] evolved to $Q^2 = 30\text{GeV}^2$ . Figure taken from [36]. . . . .	22
2.4 Simple explanation of the asymmetry in photon-nucleon scattering. The quark can only absorb a photon, if its spin is antiparallel to the photon spin. . . . .	24
2.5 Values of $g_1^d(x)$ measured by COMPASS (full circles) and SMC (open squares) for $Q^2 > 1 (\text{GeV}/c)^2$ . The curves represent the results of the fits at the $Q^2$ of the COMPASS points (solid line for all data, dashed line with COMPASS excluded). The data points are corrected for the deuterium D-wave state probability $\omega_D = 0.05$ (i.e. they correspond to the published values of $g_1^d$ divided by 0.925). . . . .	28
2.6 The quark helicity distributions $x\Delta q(x, Q^2)$ evaluated at a common value of $Q^2 = 2.5 (\text{GeV}/c)^2$ as a function of $x$ [44]. The dashed line is the GRSV2000 parametrisation (LO, valence scenario) [47] scaled with $1/(1+R)$ and the dashed-dotted line is the Blüemlein-Bottcher (BB)	

parametrisation (LO, scenario 1) [48]. Figure taken from Ref. [44]. . . . .	29
2.7 The proton structure function $F_2(x, Q^2)$ measured in electromagnetic scattering of positrons on protons at the e-p collider HERA (ZEUS and H1). . . . .	31
2.8 Schematic representation of photon-proton scattering for increasing photon virtuality $Q^2$ at fixed W. As $Q^2$ increases, the photon probes smaller transverse distance scales and is able to resolve the structure of the proton. With further increase in $Q^2$ , quarks are resolved into more quarks and gluons. . . . .	32
2.9 Feynman diagrams for the four splitting functions. The splitting function $P_{ij}$ gives the probability that a parton $i$ with momentum fraction $x$ originates from parton $j$ . . . . .	34
2.10 The AAC03 PDFs at $Q^2=1\text{GeV}^2$ are compared with the ones for other parametrisations by GRSV2000 (standard scenario) [47, 59], BB (ISET=3) [48], and LSS ( $\overline{MS}$ scheme) [60, 61, 62]. The shaded areas are the uncertainties of the AAC03 analysis. Figure taken from [43]. . . . .	38
2.11 Triangle diagram giving rise to the axial anomaly. The gluons couple via the triangle to the axial current and thus contribute to the corresponding proton matrix element. . .	39
2.12 Schematic representation of hadron production in DIS. . .	41
3.1 Typical gluon helicity distributions [90] obtained from fits to the available polarized DIS data. . . . .	51
3.2 Leading-order Feynman diagrams for di-jet production in DIS:(a) Photon-Gluon Fusion,(b) Photon-Quark Compton scattering. . . . .	52
3.3 Feynman diagrams for charm production via Photon Gluon Fusion. . . . .	56
3.4 Feynman diagrams for direct photon production. . . . .	59
4.1 The sea can be generated by the valence quarks emitting gluons which then produce pairs. . . . .	64
4.2 The proton consists of two up (UU) and one down (D) constituent quark. . . . .	65

4.3	Unpolarized functions of the valence, sea quarks and gluon plotted as function of $x$ . . . . .	73
4.4	Unpolarized functions of the gluon plotted as function of $x$ . . . . .	74
4.5	spin densities of the valence, sea quarks and gluon plotted as function of $x$ . . . . .	74
4.6	Spin density of the gluon plotted as function of $x$ . . . . .	75
4.7	Gluon polarisation $\Delta g/g$ as function of $x$ at $Q^2=Q_0^2$ obtained by NLO QCD fits (bands) and from LO analysis of hadron helicity asymmetries (symbols). It is from COMPASS QCD fits [21] including the new COMPASS deuteron data ( $Q^2=3\text{ GeV}^2$ ) . . . . .	77
4.8	$A_{  }$ for inclusive jet production at STAR as function of $p_T$ [14]. . . . .	78

---

## List of Tables

---

	<i>Page</i>
1.1 Proton and neutron properties. . . . .	3
1.2 The six quarks. . . . .	4
1.3 Current and future spin physics facilities. . . . .	9
2.1 Definition of the kinematic variables used. . . . .	13
3.1 Results from NLO fits to data for first moments of quark and gluon distributions. . . . .	50
4.1 Leading order measurements of $\Delta g/g$ . . . . .	77
4.2 Magnetic moments of proton and neutron. . . . .	81

---

## INTRODUCTION

In particle and nuclear physics the spin is an important concept, since it is related to the angular momentum, which originates in the rotational symmetry of space. The statistical property of an elementary particle is also determined by the spin, according to the Pauli principle.

The structure of the nucleon has been investigated for many years with lepton beams. Such experiments provided the basis of quantum chromodynamics, especially through the discovery of asymptotic freedom. The discovery potential of the hadron colliders would have never been so promising without a detailed knowledge of the nucleon structure.

The mass of the nucleon cannot be explained by the bare quark masses. Instead most of the mass is due to the field energy of the quarks and gluons. When the fractional momentum  $x$ , carried by the quarks, is integrated, it comes to only  $\sim 50\%$  of the total momentum. The rest of the momentum is carried by the gluons. This is referred to as the momentum sum rule.

Since the surprising EMC measurement [1] of the polarized structure function of the proton  $g_1^p(x, Q^2)$  was reported more than seventeen years ago, the spin structure of the proton remains a problem. As is well known, a proton is a composite particle. Its spin is carried by its constituents, as described by the sum rule,

$$\frac{1}{2} = \frac{1}{2} \Delta \Sigma + \Delta G + \langle L_z \rangle_{q+g} \quad (1)$$

where  $\frac{1}{2}$  on the left side means a spin of the proton, while  $\Delta \Sigma$ ,  $\Delta G$  and  $\langle L_z \rangle_{q+g}$  represent the amount of the proton spin, carried by the

constituent quarks, gluons and their orbital angular momenta respectively. A study of the polarized structure functions of the nucleon gives information about the valence quark distributions in the proton. However, the knowledge on  $\Delta g$  and  $\langle L_z \rangle_{q+g}$  is still poor, because it is very difficult to extract information from the existing experimental data. In this work we are interested in the polarized gluon distribution  $\Delta g$ . To extract information about it, many processes, depending on the gluon interactions, have been proposed and studied.

The fractional quark-spin contribution  $\Delta\Sigma$  is found to be 0.1 – 0.3 from lepton scattering data, combined with the  $\beta$  decay constants of the baryons. This is significantly smaller than the naive expectation. The proton spin is related to the number of flavors at infinite 4-momentum squared[2]:

$$\frac{1}{2}\Delta\Sigma + L_q = \frac{1}{2} \frac{3n_f}{3n_f + 16} \quad ; \quad \Delta g + L_g = \frac{1}{2} \frac{16}{3n_f + 16} \quad (2)$$

Each term corresponds to 0.136–0.18 and 0.364–0.32, respectively depending on the number of flavors  $n_f=2(3)$ . Once  $\Delta g$  is measured to a reasonable precision, then we will know roughly, how the spin of the proton is distributed to each component.

The spin sum rule eq. (1) concerns the longitudinal spin structure of the proton. We concentrate on the gluon polarization in this thesis.

# CHAPTER 1

## The nucleon

### 1.1 What do we know about the nucleon?

The proton is the only stable baryon. The neutron is the partner of the proton. The two main differences are: the neutron has no charge, it is heavier and decays into a proton. A free neutron decays in approximately 15 minutes. However, when bound in a non-radioactive nucleus, the neutron is stable and like the proton does not decay. Table(1.1) summarizes the properties of the proton and neutron.

Table(1.1) Proton and neutron properties:

	Proton	Neutron
Mass	938.27 MeV	939.6 MeV
Charge	+1	0
Spin	1/2	1/2
Lifetime	$> 10^{32}$ years	885.7 seconds

Our present understanding is that the proton and neutron have complex internal structures consisting of quarks of different flavors and of gluons, described by QCD. Relating the simple external properties of the proton and neutron to the internal structure remains one of the challenges in physics today.

Table(1.2) gives the six quarks, that have been found in nature, and their charge. The only known difference between the quarks of the same charge and different generations is their mass. For the proton structure, it is actually the lightest quarks, up and down, that play the leading role.

In the most naive model of the proton, the proton consists of two up quarks and one down quark bound together. To get a neutron, one simply

interchanges the up quarks with the down quarks, yielding a zero charge object. From neutrino and electron scattering experiments it is known that the structure of the proton is more complicated. In the proton there are also sea quarks and sea anti-quarks as well as gluons, that are the mediators of the strong interaction:

$$proton = valence\ quarks + sea\ quarks + gluons$$

We are trying to find out, what fraction of the proton spin is carried by the quarks and what fraction is carried by the gluons.

Table(1.2) The six quarks:

generation \ charge	1 <sup>st</sup>	2 <sup>st</sup>	3 <sup>st</sup>
Q= +2/3	up	charm	top
Q= -1/3	down	strange	bottom

## 1.2 The substructure of the nucleon

The first polarized electron scattering experiment was performed at the Stanford Linear Accelerator Center (SLAC) in California. Soon afterwards a muon scattering experiment was done at CERN, and a second electron scattering experiment was built at DESY in Hamburg, Germany.

In order to present and interpret the results from these experiments, it is necessary to introduce the formalism. One measures an asymmetry and extracts an asymmetry  $A_1$  :

$$A_1 = \frac{N_{\uparrow\downarrow} - N_{\uparrow\uparrow}}{N_{\uparrow\downarrow} + N_{\uparrow\uparrow}} \quad (1.1)$$

Here  $N_{\uparrow\downarrow}$  corresponds to the number of electrons counted in the detector with the beam and target spins aligned anti-parallel to one

another, and  $N\uparrow\uparrow$  corresponds to the case, where the spins are aligned.

From this asymmetry we find the proton or neutron spin structure function,  $g_1^P$  or  $g_1^n$ , where,

$$g_1 \approx A_1 \cdot F_1 \quad (1.2)$$

for a proton or a neutron. The function  $F_1$  is a quantity, which is measured in unpolarized scattering experiments. We have to introduce the structure function  $g_1$ , since it is the quantity, that is directly related to the quark contribution of the proton and neutron spin.

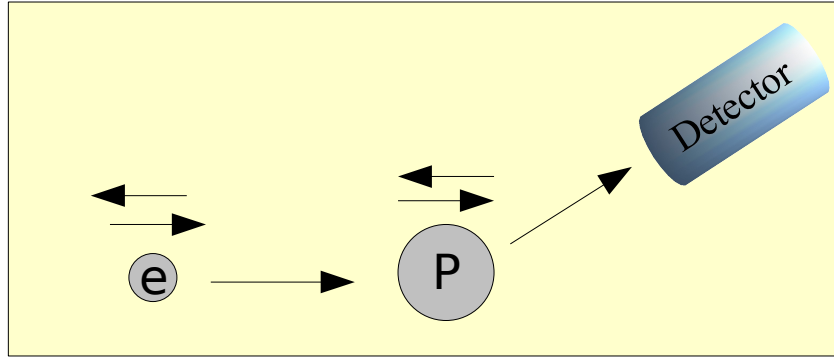


Figure 1.1 Scheme of a polarized electron-polarized proton scattering experiment

In the naive parton model the integral over  $g_1^P$  can be written as follows:

$$\int_0^1 dx g_1^P(x, Q^2) = \frac{1}{2} \left[ \frac{4}{9} \Delta u + \frac{1}{9} \Delta d + \frac{1}{9} \Delta s \right] \quad (1.3)$$

where  $\Delta u$ ,  $\Delta d$  and  $\Delta s$  are, respectively, the individual up, down and strange quark contributions to the proton and neutron spin. More information is actually needed to extract the total quark contribution

$$\Delta \Sigma = \Delta u + \Delta d + \Delta s$$

Let's assume for simplicity, that the proton is made up of two up quarks and one down quark, and the neutron is made up of two down quarks and an up quark. Figure(1.2) presents this model of the proton and neutron. If one takes all combinations of three quark states, the polarized proton wave function can be written as:

$$|p\uparrow\rangle = 2|u\uparrow u\uparrow d\downarrow\rangle + 2|u\uparrow d\downarrow u\uparrow\rangle + 2|d\downarrow u\uparrow u\uparrow\rangle - |u\uparrow u\downarrow d\uparrow\rangle - |u\uparrow d\uparrow u\downarrow\rangle - |d\uparrow u\uparrow u\downarrow\rangle - |u\downarrow u\uparrow d\uparrow\rangle - |u\downarrow d\uparrow u\uparrow\rangle - |d\uparrow u\uparrow u\downarrow\rangle \quad (1.4)$$

The polarized proton with spin pointed up will look like one of the two objects Figure(1.3), with the left object occurring 2/3 of the time, and the right object occurring 1/3 of the time. If one scatters an electron off a polarized proton, 2/3 of the time the electron will see the left object and 1/3 of the time it will see the right object.

If one wants to know what is the probability that the electron will scatter off an up quark with spin up, then one has to count the probability of hitting the left or right object times the probability that the electron will scatter off an up quark with spin up. The answer is

$$P(u\uparrow) = \frac{2}{3} \cdot \frac{2}{3} + \frac{1}{3} \cdot \frac{1}{3} = \frac{5}{9} \quad (1.5)$$

The first 2/3 comes from hitting the left object, the second 2/3 comes from the probability of hitting an up quark with spin up in the left object, the next 1/3 comes from the probability of hitting the right object and the last 1/3 comes from the probability of hitting an up quark with spin up in the right object.

One can calculate the probability of finding each type of polarized quark, and the results are:

$$P(u\uparrow) = 5/9 \quad , \quad P(u\downarrow) = 1/9 \quad , \quad P(d\uparrow) = 1/9 \quad , \quad P(d\downarrow) = 2/9$$

The sum of all the above probabilities is one, as expected.

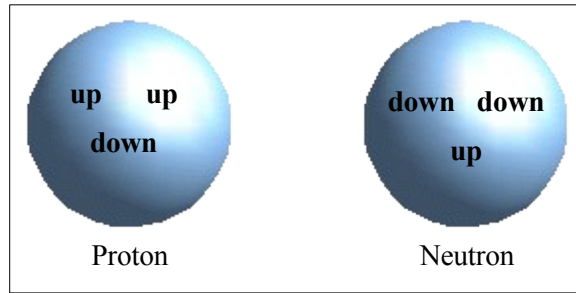


Figure 1.2 Simplest quark model of the proton and neutron.

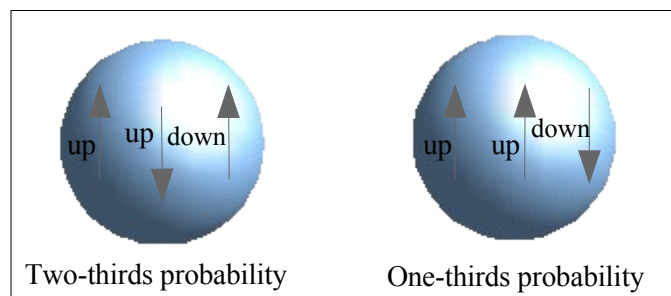


Figure 1.3 Simplest quark model of a polarized proton.

The last step is to calculate the asymmetry  $A_1$ . One has to multiply the charge squared of the quark times the probability of the quark being spin up minus spin down and then divide by the sum of the quark probabilities:

$$A_1^p = \frac{\frac{4}{9}[p(u\uparrow) - p(u\downarrow)] + \frac{1}{9}[p(d\uparrow) - p(d\downarrow)]}{\frac{4}{9}[p(u\uparrow) + p(u\downarrow)] + \frac{1}{9}[p(d\uparrow) + p(d\downarrow)]} \quad (1.6)$$

One finds  $A_1^p = 5/9$ , which is a large asymmetry!

If one wants to calculate the same quantity for the neutron, one has to interchange the up quark probability with the down quark probability, and one finds  $A_1^n = 0$ .

## 1.3 EXPERIMENTAL ASPECTS

In the experiments with polarized beams the spin dependent asymmetry in the cross section for lepton scattering is measured, from which the spin dependent structure function of the proton  $g_1(x)$  is deduced. Here  $x$  is the fraction of the momentum of the proton carried by the struck quark. The integral of  $g_1(x)$  over  $x$  is used to test the Ellis-Jaffe sum rule [3] and to investigate the contribution of the spin of the quarks to the proton spin.

There are many experimental efforts triggered by the “spin crisis”. Ongoing and future experiments are summarized in Table(1.3). The experimental data to determine the spin structure of the nucleon so far are dominated by the lepton scattering data on fixed targets. The efforts are being extended to cover various reactions using  $pp$  and  $ep$  colliders and the first polarized  $pp$  collider, RHIC. Future facilities will cover an extended  $x$ -range. Elastic scattering  $\nu N \rightarrow \nu N$  [4] could provide the first moment of the polarized strange quark distribution  $\Delta s$ .

These experimental facilities utilize different ways to pin down the spin structure. Each way has its advantages and disadvantages. As we are going to see below, it is important to use all possibilities to obtain a comprehensive picture of the spin structure.

### 1.3.1 Electromagnetic interaction

The classical probe in the study of substructure is the electromagnetic interaction. A lepton scattering interaction is well understood and precisely calculable. There are many advantages of these reactions, including the clear definition of the kinematics, which requires only the

four-momenta of the incoming and outgoing lepton. It is sensitive to the electric charges of the quarks. The gluons would appear only in a sub-leading contribution. This type of measurement has been done at CERN (COMPASS), DESY (HERMES), and J-Lab.

Higher energy machines are planned at J-Lab (ELIC) and at BNL (eRHIC). Drell-Yan production of lepton pairs will be studied at RHIC. An experiment at GSI (PAX) is planned to use  $\bar{P}\uparrow P\uparrow$  collisions to measure the transversity distributions in the nucleon.

Table(1.3) Current and future spin physics facilities:

Experiment	Reaction	Beam energies	Status
HERMES at DESY	$e^\pm p, d$	$E_e = 27$ GeV fixed target	ended in summer 2007
COMPASS at CERN	$\mu p, d$	$E_\mu = 160$ GeV fixed target	Data Taking
RHIC-Spin at BNL	$pp$	$\sqrt{s} = 200,500$ GeV collider	continuing
J-Lab	$e^- N$	$E_e \sim 5$ GeV fixed target	continuing
eRHIC at BNL	$e^- p$	$\sqrt{s} = 100$ GeV collider	planned
12 GeV upgrade at J-Lab	$e^- N$	$E_e = 12$ GeV fixed target	planned
ELIC at J-Lab	$e^- p$	$\sqrt{s} = 20-65$ GeV collider	planned
J-PARC	$pp, pA$	$E_p = 50$ GeV fixed target	under construction
GSI-FAIR	$\bar{p} p$	$\sqrt{s} \sim 15$ GeV collider	planned
FINeSSE	$\nu N$ elastic	$E_\nu = 1$ GeV fixed target	proposed

### 1.3.2 The strong Interaction

Until recently the gluon contribution to the spin structure of the nucleon has been poorly known. It can be measured by experiments, using the strong interaction. The leading processes are  $gg$ ,  $gq$  and  $qq$  scattering. The  $gg$  and  $gq$  -processes dominate in the lower  $P_T$  region where the statistics is high. The STAR experiment at RHIC presented their recent results on  $A_{LL}$  for jet production in pp collision at  $\sqrt{s}=200\text{ Gev}$  from Run-3 (2003)[5]. The PHENIX experiment also reported their newly obtained  $A_{LL}$  for  $\pi^0$  production in Run-5[6].

A good way to measure the gluon polarization is prompt photon production, which is dominated by the gluon Compton process,  $gq \rightarrow \gamma q$ . It is being explored in HERMES and COMPASS. Here the real/virtual photon and gluon fuse into a  $\bar{q}q$  pair (photon-gluon fusion). The current experimental data allow to say something about the gluon polarization  $\Delta g/g(x)$ .

### 1.3.3 The weak interaction

A missing information is the flavor separation, which can be done using the weak interaction. The  $W$  production in  $pp$  collisions is a pure  $V-A$  process, where only left-handed quark and right-handed anti-quark can contribute. It is an ideal place to study the spin structure. The  $W$  couples to the weak charge, which is highly correlated with the flavor.

Such a measurement can be done at RHIC, when it reaches its highest energy  $\sqrt{s}=500\text{ Gev}$ ; in 2005 one had  $\sqrt{s}=410\text{ Gev}$ .

## CHAPTER 2

### Theoretical framework

#### 2.1 The Gluon in the Nucleon and the Gluon Polarisation

The gluon contribution to the spin of the nucleon is still not known. The gluons do not couple to the photon and thus cannot be accessed directly in the leading order deep inelastic scattering (DIS) process. But they contribute to the cross section due to higher order QCD processes.

The gluon distribution can be obtained indirectly from the scaling violations of the quark distributions using the evolution equations. Alternatively the higher order processes can be separated experimentally, and the unpolarised gluon density can be determined directly. Compared to the unpolarised case, the data on polarised experiments cover a relatively small kinematic range. Therefore it is extremely difficult to obtain an accurate gluon helicity contribution, and a direct measurement of the gluon polarisation  $\Delta G/G$  is needed. The direct measurement can either be done in deep inelastic scattering, as performed by COMPASS, or in polarised p-p collisions, a method followed at the Relativistic Heavy Ion Collider (RHIC). A more detailed treatment of the underlying polarised and unpolarised physics and experimental results can be found in the review articles [19-22].

#### 2.2 Deep inelastic scattering

In a deep inelastic scattering experiment an incoming beam of leptons with energy  $E$  scatters off a fixed hadronic target. The energy and direction of the scattered lepton are measured in the detector, but the final hadronic state (denoted by  $X$ ) is not measured. The lepton interacts with

the target through the exchange of a virtual photon. The target hadron absorbs the virtual photon to produce the final state X. If the hadron remains intact, the process is an elastic scattering. In the deep inelastic region the cross section can be expressed in terms of the structure functions. I will only discuss the case of fixed-target deep inelastic scattering in detail.

The basic diagram for the deep inelastic scattering is shown schematically in fig. 2.1 There are numerous kinematic variables, which are used in the discussion of deep inelastic scattering (see Table 2.1).

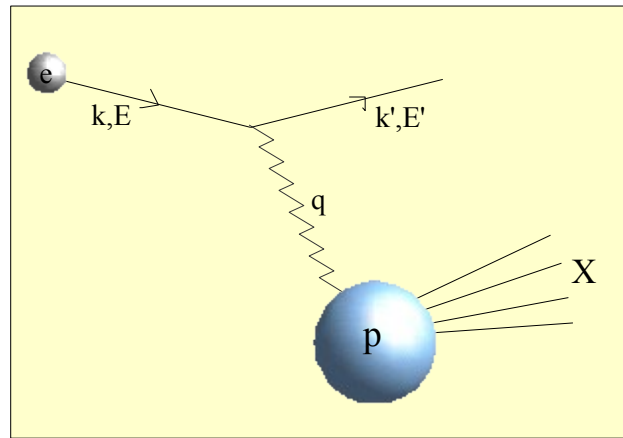


Figure 2.1 The basic diagram for deep inelastic lepton hadron scattering.

### 2.2.1 The formalism of polarized deep inelastic scattering

The difference in the cross sections for deep inelastic scattering of leptons, polarized antiparallel and parallel to the spin of the proton, can be written in the single photon exchange approximation as:

$$\frac{d^2\sigma_{\uparrow\downarrow}}{dQ^2 d\nu} - \frac{d^2\sigma_{\uparrow\uparrow}}{dQ^2 d\nu} = \frac{4\pi\alpha^2}{E^2 Q^2} [M(E + E' \cos \theta) G_1(Q^2, \nu) - Q^2 G_2(Q^2, \nu)] \quad (2.1)$$

Table 2.1 Definition of the kinematic variables used.

$M$	The mass of the target hadron. e.g. a proton or neutron.
$m$	Lepton mass.
$E$	The energy of the incident lepton.
$E'$	The energy of the scattered lepton.
$K=(E, \vec{K})$	The four momentum of the initial lepton. $k = (E, 0, 0, E)$ , if the lepton mass is neglected.
$K'=(E', \vec{K}')$	The four momentum of the scattered lepton.
$P=(M, \vec{0})$	The four momentum of target proton.
$s=\frac{1}{m}(k, 0, 0, E)$	Lepton spin four vector.
$S=(0, \vec{S})$	Proton spin four vector.
$q=k-k'=(\nu, \vec{q})$	The four momentum transfer in the scattering process, i.e. the momentum of the virtual photon.
$Q^2=-q^2 \approx 4EE' \sin^2(\theta/2)$	negative virtual photon 4-momentum squared.
$\nu=\frac{P \cdot q}{M}=E-E'$	The energy of the virtual photon (the energy loss of the lepton).
$y=\frac{\nu}{E}=\frac{p \cdot q}{p \cdot k}$	the fractional energy loss of the lepton.
$\theta$	Scattering angle in the laboratory.
$x=\frac{Q^2}{2M\nu}$	Bjorken scaling variable.

The scaling variable  $x$  was first introduced by Bjorken[33] and is crucial to understand deep inelastic scattering. QCD predicts that the structure functions are functions of  $x$  and are independent of  $Q^2$  to leading order, a property known as scaling. The scaling has been proposed by

Bjorken[33]. Higher order corrections in QCD produce a small logarithmic  $Q^2$  dependence of the structure functions, which is calculable for large  $Q^2$ , since QCD is an asymptotically free theory. Deep inelastic scattering is the study of lepton-hadron scattering in the limit:  $x$  fixed,  $Q^2 \rightarrow \infty$ .

The functions  $G_1(Q^2, \nu)$  and  $G_2(Q^2, \nu)$  in equation (2.1) are the spin dependent structure functions of the target nucleon. In the scaling limit these structure functions are expected to become functions of  $x$  [9] :

$$\begin{aligned} M^2 \nu G_1(Q^2, \nu) &\rightarrow g_1(x), \\ M \nu^2 G_2(Q^2, \nu) &\rightarrow g_2(x) \end{aligned} \quad (2.2)$$

These structure functions can be obtained from the experiments, in which longitudinally polarized leptons are scattered from longitudinally polarized target nucleons. One measures the asymmetry

$$A = \frac{d\sigma^{\uparrow\downarrow} - d\sigma^{\uparrow\uparrow}}{d\sigma^{\uparrow\downarrow} + d\sigma^{\uparrow\uparrow}} \quad (2.3)$$

This asymmetry is related by the optical theorem to the virtual photon asymmetries  $A_1$  and  $A_2$ ,

$$A = D(A_1 + \eta A_2) \quad (2.4)$$

where

$$A_1 = \frac{\sigma_{1/2} - \sigma_{3/2}}{\sigma_{1/2} + \sigma_{3/2}}, \quad (2.5)$$

$$A_2 = \frac{\sigma_{TL}}{\sigma_T}, \quad (2.6)$$

$$D = \frac{y(2-y)}{y^2 + 2(1-y)(1+R)} \quad (2.7)$$

$$\eta = \frac{2(1-y)}{y(2-y)} \frac{\sqrt{Q^2}}{E} \quad (2.8)$$

Here  $\sigma_{1/2}(\sigma_{3/2})$  is the virtual photoabsorption cross section. The projection of the total angular momentum of the photon-nucleon system along the incident lepton direction is  $1/2$  ( $3/2$ ).  $\sigma_T = 1/2(\sigma_{1/2} + \sigma_{3/2})$  is the total transverse photoabsorption cross section, and  $\sigma_{TL}$  is a term arising from the interference between transverse and longitudinal amplitudes. The term  $R$  in equation (2.7) is the ratio of the longitudinal to transverse photoabsorption cross sections, and  $D$  can be regarded as a depolarization factor of the virtual photon.

The asymmetries  $A_1$  and  $A_2$  can be expressed in terms of the structure functions  $g_1$  and  $g_2$  [10] as ,

$$A_1 = (g_1 - \nu^2 g_2) \frac{1}{F_1} \quad (2.9)$$

$$A_2 = \nu(g_1 - g_2) \frac{1}{F_1} \quad (2.10)$$

Here  $F_1$  is the spin independent structure function of the proton, and  $\nu^2 = Q^2/\nu^2$ . Eliminating  $g_2$ , we obtain to first order in  $\nu$ ,

$$g_1 = F_1(A_1 + \nu A_2) \quad (2.11)$$

Substituting for  $A_1$  from (2.4) gives

$$g_1 = F_1 \left( \frac{A}{D} + (\nu - \eta) A_2 \right) \quad (2.12)$$

There are rigorous positivity limits on the asymmetries [11] i.e.  $|A_1| \leq 1$  and  $|A_2| \leq \sqrt{R}$ , since  $\nu$ ,  $\eta$  and  $R$  all small in the kinematic range of this experiment. The term in  $A_2$  may be neglected.

$$A_1 \simeq \frac{A}{D} \quad (2.13)$$

$$g_1 \simeq A_1 F_1 = \frac{A_1 F_2}{2x(1+R)} \quad (2.14)$$

Here  $F_2$  is the second spin independent proton structure function. Neglecting  $A_2$  is equivalent to neglecting the contribution of  $g_2$  which has been shown to have a negligible effect [12].

The structure function  $g_1(x)$  is obtained as follows. The asymmetry  $A$  (equation (2.3)) is obtained from the experimental data. The virtual photon asymmetry  $A_1$  is deduced via equation (2.13). The structure function  $g_1(x)$  is obtained from equation (2.14), using the known values of  $F_2$  and  $R$ . The effect of neglecting  $A_2$  is included in the systematic error, using the above mentioned limits for  $A_2$ .

### 2.2.2 Theoretical models

By angular momentum conservation a spin  $\frac{1}{2}$  parton cannot absorb a photon, when their two helicities are parallel. Hence in the quark-parton model (QPM),  $\sigma_{1/2}(\sigma_{3/2})$  can only receive contributions from partons, whose helicities are antiparallel (parallel) to that of the nucleon. It follows:

$$A_1 = \frac{\sigma_{1/2} - \sigma_{3/2}}{\sigma_{1/2} + \sigma_{3/2}} = \frac{\sum e_i^2 (q_i^+(x) - q_i^-(x))}{\sum e_i^2 (q_i^+(x) + q_i^-(x))} \quad (2.15)$$

Here  $q_i^{+(-)}(x)$  is the distribution function for the quarks of flavour  $i$  and charge number  $e_i$ , whose helicities are parallel (antiparallel) to that of the nucleon. The sum is over all quark flavours  $i$ . In this model  $F_1$  is

given by

$$F_1(x) = \frac{1}{2} \sum e_i^2 (q_i^+(x) + q_i^-(x)) \quad (2.16)$$

From equations (2.14) and (2.15) follows:

$$g_1(x) = \frac{1}{2} \sum e_i^2 (q_i^+(x) - q_i^-(x)) \quad (2.17)$$

In the simple non-relativistic QPM, in which the proton consists of three valence quarks in an SU(6) symmetric wave function, one has  $A_1^p = \frac{5}{9}$  and  $A_1^n = 0$ . Thus  $A$  is independent of  $x$ . Such a model clearly does not describe the SLAC data. Many models, mainly based on the QPM, were developed to predict the behaviour of the asymmetry  $A_1$ . Models giving a good representation of the SLAC data were developed by Cheng and Fischbach [13] and Callaway and Ellis [14]. These incorporate the perturbative QCD prediction [15] that  $A_1$  tends to unity as  $x$  approaches unity.

### 2.2.3 Sum rules in polarised deep inelastic scattering

A sum rule, derived by Bjorken [49] from current algebra, relates the integral over all  $x$  of the difference of  $g_1$  for the proton and neutron to the ratio of the axial vector to vector coupling constants in nucleon beta decay, denoted by  $g_A$ . In the scaling limit it can be written,

$$\int_0^1 dx [g_1^p(x, Q^2) - g_1^n(x, Q^2)] = \frac{1}{6} g_A \left(1 - \frac{\alpha_s}{\pi}\right) \quad (2.18)$$

where the factor  $(1 - \frac{\alpha_s}{\pi})$  arises from QCD radiative corrections [18].

Separate sum rules for the proton and the neutron were derived by

Ellis and Jaffe [16] in a more model dependent approach. Assuming an exact flavour SU(3) symmetry in the baryon-octet decays and neglecting the net polarization of the strange quark sea of the nucleon, they derived

$$\int_0^1 dx g_1^p(x, Q^2) = \frac{g_A}{12} \left[ +1 + \frac{5}{3} \frac{3F/D-1}{F/D+1} \right] \quad (2.19)$$

$$\int_0^1 dx g_1^n(x, Q^2) = \frac{g_A}{12} \left[ -1 + \frac{5}{3} \frac{3F/D-1}{F/D+1} \right]$$

where  $F$  and  $D$  are the antisymmetric and symmetric SU(3) couplings. Applying QCD radiative corrections, one obtains[18]:

$$\int_0^1 dx g_1^{p(n)}(x, Q^2) = \frac{g_A}{12} \left[ \pm \left( 1 - \frac{\alpha_s}{\pi} \right) + \frac{1}{3} \frac{3F/D-1}{F/D+1} \left[ 5 - \left( 1 + 4 \frac{33-8n_f}{33-2n_f} \right) \frac{\alpha_s}{\pi} \right] \right]$$

(  $n_f$  : the number of quark flavours).

### 2.3 Interpretation in the Quark Parton Model

In 1964 the quark model was proposed by Gell-Mann [25] and Zweig [26]. Feynman developed in 1969 the Quark Parton Model (QPM) to provide a simple physical picture of the observed scaling behaviour [27, 28]. In this model the nucleon is made up of pointlike constituents, known as partons. The charged partons, carrying fractions of the elementary charge  $e$  and spin  $1/2$ , were later identified as the quarks. The electrically neutral spin 1 partons, which do not interact with the virtual photon, are the gluons. The QPM is formulated in the infinite momentum frame, where the target nucleon moves with  $p \rightarrow \infty$ . The rest masses and the transverse momenta of the partons are neglected. During the time, in which the virtual photon interacts with the quark, it is essentially a free

particle, not interacting with the other partons in the nucleon. In a good approximation the structure of the nucleon can then be described by the longitudinal momenta of its components. In the infinite momentum frame the interpretation of the Bjorken scaling variable  $x$  as momentum fraction of the nucleon, carried by the struck parton, becomes exact.

### 2.3.1 The distributions of Partons

The scattering process off a nucleon can be described as an incoherent sum of the interactions of the virtual photon with the partons. The single interaction can be interpreted as an elastic scattering. The cross section of a lepton scattering off a pointlike quark of flavour  $f$ , that carries a momentum fraction  $x_f$  of the nucleon, can be calculated in QED. By comparing the cross section for inelastic scattering with the one for elastic scattering, the structure functions for a single pointlike parton are [29] :

$$2 F_1^{point}(\nu, Q^2) = e_f^2 \frac{Q^2}{2m} \delta\left(\nu_p - \frac{Q^2}{2m}\right) = e_f^2 \delta\left(x_f - \frac{Q^2}{2M\nu}\right) \quad (2.20)$$

$$F_2^{point}(\nu, Q^2) = e_f^2 \nu \delta\left(\nu_p - \frac{Q^2}{2m}\right) = e_f^2 x_f \delta\left(x_f - \frac{Q^2}{2M\nu}\right) \quad (2.21)$$

Here  $m$  is the mass of the parton,  $e_f$  its charge,  $\nu_p = (p_{parton} \cdot q)/m$  with

$p_{parton} = x_f P$  being the parton momentum, which is the fraction  $x_f$  of the nucleon momentum  $P$ , and  $Q^2/2M\nu = x$  is the Bjorken variable. Thus  $x$  has to be equal to  $x_f$ , and the virtual photon can only be absorbed by the quark with the right momentum fraction. Summing over all quarks and antiquarks in the nucleon gives

$$F_2(x) = \sum_f \int dx_f e_f^2 q_f(x_f) x_f \delta(x_f - x) \quad (2.22)$$

where the  $q_f(x)$  are the parton distribution functions. The differential  $q_f(x)dx$  is the probability to find a quark of flavour  $f$  with a momentum fraction in the range  $x, x+dx$ . This leads to the following form of the structure functions:

$$F_2(x) = x \sum_f e_f^2 (q_f(x) + \bar{q}_f(x)) \quad (2.23)$$

With  $F_2 = 2xF_1$  we obtain:

$$F_1(x) = \frac{1}{2} \sum_f e_f^2 (q_f(x) + \bar{q}_f(x)) \quad (2.24)$$

The sum runs over all quarks inside the nucleon (the valence quarks carrying the quantum numbers of the nucleon, and the sea quarks).

From the parton distributions one can obtain the number densities of the quarks inside the nucleon. For a proton we find the sum rules:

$$\int_0^1 [u(x) - \bar{u}(x)] dx = \int_0^1 u_v(x) dx = 2 \quad (2.25)$$

$$\int_0^1 [d(x) - \bar{d}(x)] dx = \int_0^1 d_v(x) dx = 1 \quad (2.26)$$

$$\int_0^1 [s(x) - \bar{s}(x)] dx = 0 \quad (2.27)$$

Here  $u_v(x)$  and  $d_v(x)$  are the valence quark distributions. Their integral corresponds to the number of quarks in the static picture of the nucleon, where the proton is composed of two up- and one down-quark. The distributions for the neutron can be obtained using isospin symmetry (exchanging  $u$ - and  $d$ -quarks):

$$u^p(x) \equiv d^n(x) \quad , \quad d^p(x) \equiv u^n(x) \quad , \quad s^p(x) \equiv s^n(x) \quad (2.28)$$

The integral  $\int_0^1 dx x q(x)$  gives the fraction of the total momentum of the nucleon that is carried by all quarks:

$$\int_0^1 dx x [u(x) + \bar{u}(x) + d(x) + \bar{d}(x) + s(x) + \bar{s}(x)] = 1 - \varepsilon_g \quad (2.29)$$

where  $\varepsilon_g = \frac{p_{gluon}}{p_{proton}}$  is the momentum fraction carried by neutral partons, which are not directly probed by the photon. It turns out that about half of the proton's momentum is carried by the charged partons, the remaining constituents interact neither electromagnetically nor weak (as known from neutrino scattering experiments). They are identified with the gluons.

The analysis of inclusive and semi-inclusive DIS experiments using hadron identification with electron, muon and neutrino beams on proton and deuteron targets allows to disentangle the contributions from the various types of quarks. Fig.2.2 shows the parametrisation of valence, sea-quark and gluon distributions using these data. At HERA the gluon distribution has also been measured directly using methods analog to the determination of the polarised gluon density. Fig.2.3 shows one of the measurements done by H1 using multi-jet events from boson-gluon fusion in deep inelastic scattering. The gluon density increases with decreasing fractional momenta of the gluons, as expected in the theory of QCD.

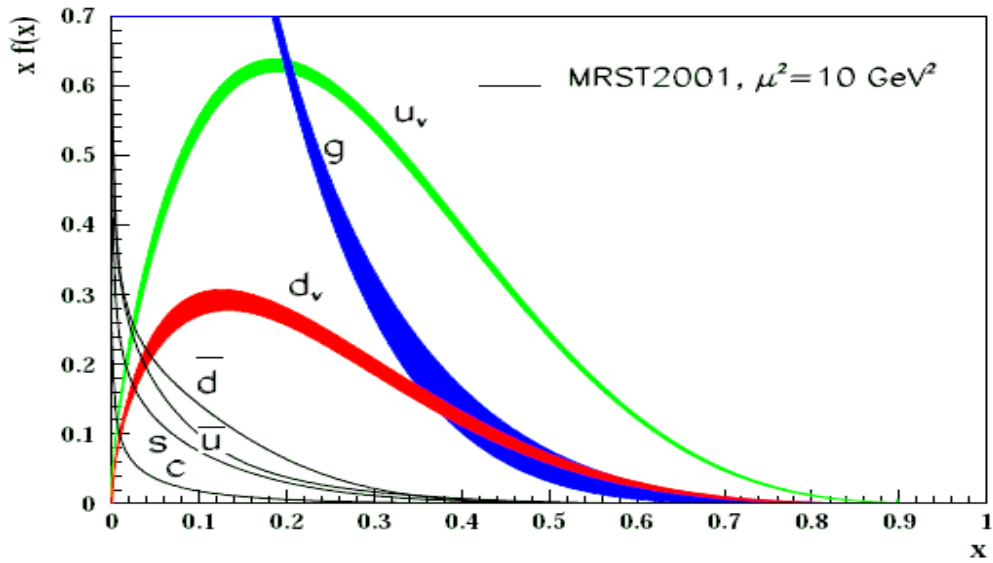


Figure 2.2: Distributions of  $x$  times the unpolarised parton distributions  $f(x)$  (where  $f = u_v, d_v, \bar{u}, \bar{d}, s, c, g$ ) using the MRST2001 parametrisation [30, 31] (with uncertainties for  $u_v, d_v$  and  $g$ ) at a scale of  $10\text{GeV}^2$ . Figure taken from [32].

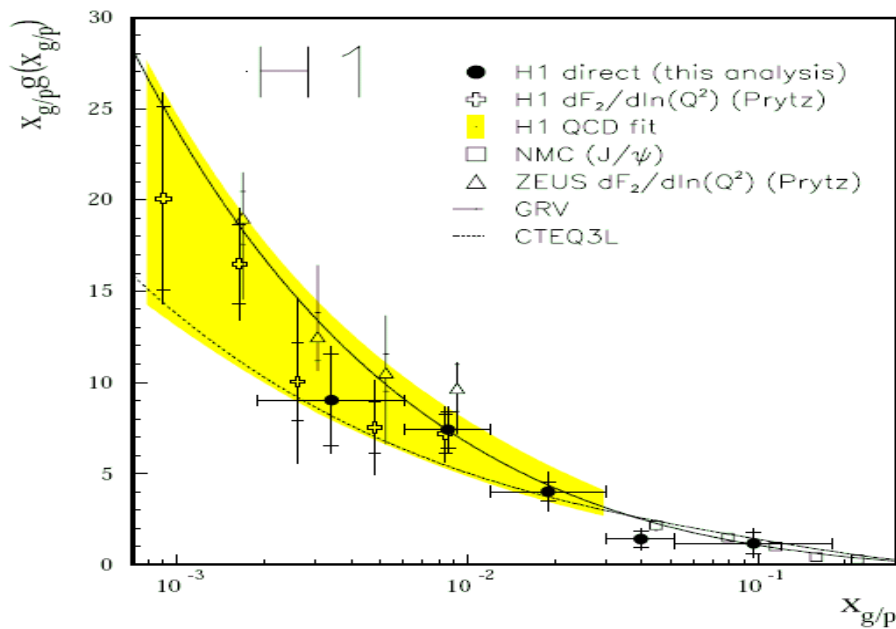


Figure 2.3: Direct determination of the gluon distribution at HERA. The measured gluon density at an average  $Q^2$  of  $30\text{GeV}^2$  is compared with the indirect determinations by H1 [33] and ZEUS [34] at  $Q^2 = 20\text{GeV}^2$ , and with a determination from  $J/\Psi$  production by NMC [35] evolved to  $Q^2 = 30\text{GeV}^2$ . Figure taken from [36].

### 2.3.2 The Spin of the Nucleon and the first Moment of $g_1$

The polarised structure function  $g_1$  can be written as follows:

$$g_1(x, Q^2) = \frac{1}{2} \sum_f e_f^2 (\Delta q_f(x) + \Delta \bar{q}_f(x)) \quad (2.30)$$

Here

$$\Delta q_f(x) = q_f^+(x) - q_f^-(x) \quad (2.31)$$

and  $(q^-)$   $q^+$  are the number densities of quarks with momentum fraction  $x$  of the parent nucleon momentum  $P$  and spin (anti-)parallel to the parent nucleon spin. The unpolarised parton densities are:

$$q_f(x) = q_f^+(x) + q_f^-(x) \quad (2.32)$$

The structure function  $g_1$  can be determined by a measurement of  $A_1$  via Eq.(2.14). A photon with a positive helicity can, due to angular momentum conservation, only be absorbed by a quark with negative helicity, since the final state, a quark, has spin 1/2 and cannot have spin 3/2 (Fig.2.4). If the helicity of the parent nucleon is opposite to the photon helicity, one probes the distribution  $q^+(x)$ , while the distribution  $q^-(x)$  is probed, when photon and nucleon have the same helicity. For  $g_2$  there is no simple interpretation in the quark parton model.

Information about  $g_1(x, Q^2)$  for all  $x$  gives information about the quark helicity contribution to the nucleon spin. The first moment of  $g_1$  is given by:

$$\Gamma_1 = \int_0^1 g_1(x) dx = \frac{1}{2} \sum_f e_f^2 \int_0^1 [\Delta q_f(x) + \Delta \bar{q}_f(x)] dx, \quad (2.33)$$

with

$$\Delta q_f = \int_0^1 [\Delta q_f(x) + \Delta \bar{q}_f(x)] dx$$

$$\Gamma_1 = \frac{1}{2} \sum_f e_f^2 \Delta q_f \quad (2.34)$$

For the proton (neglecting the contributions from heavy quarks), one obtains

$$\begin{aligned} \Gamma_1^p &= \frac{1}{2} \left( \frac{4}{9} \Delta u + \frac{1}{9} \Delta d + \frac{1}{9} \Delta s \right) \\ &= \frac{1}{12} (\Delta u - \Delta d) + \frac{1}{36} (\Delta u + \Delta d - 2\Delta s) + \frac{1}{9} (\Delta u + \Delta d + \Delta s) \end{aligned} \quad (2.35)$$

In the naive parton model the quantity

$$\Delta \Sigma = \Delta u + \Delta d + \Delta s \quad (2.36)$$

gives the helicity contribution of the quarks to the nucleon spin.

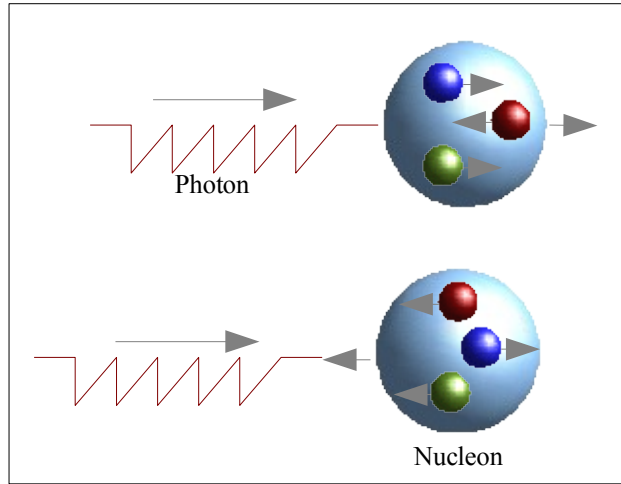


Figure 2.4: Simple explanation of the asymmetry in photon-nucleon scattering. The quark can only absorb a photon, if its spin is antiparallel to the photon spin.

Using the operator product expansion (OPE), one can connect the three terms in Eq. (2.35) to the expectation values  $a_j$  of the proton matrix elements of the SU(3) flavour octet of quark axial-vector currents [19]. The  $a_j$  are given by:

$$\langle P, S | J_{5\mu}^j | P, S \rangle = M a_j S_\mu, \quad j=1\dots 8 \quad (2.37)$$

$$J_{5\mu}^j = \bar{\Psi} \gamma_\mu \gamma_5 \frac{\lambda_j}{2} \Psi \quad (2.38)$$

The  $\lambda_j$  are the Gell-Mann matrices, and  $\Psi$  is a column vector in flavour space:

$$\Psi = \begin{bmatrix} \psi_u \\ \psi_d \\ \psi_s \end{bmatrix} \quad (2.39)$$

The matrix element  $a_0$  describes the flavour singlet operator

$$J_{5\mu}^0 = \bar{\Psi} \gamma_\mu \gamma_5 \Psi \quad (2.40)$$

One finds:

$$\langle P, S | J_{5\mu}^0 | P, S \rangle = M a_0 S_\mu \quad (2.41)$$

The octet of currents is conserved. Therefore the numbers  $a_j$ ,  $j=1\dots 8$  are independent of  $Q^2$ . The singlet current  $a_0$  is not conserved, i.e. depends on  $Q^2$ . This is a consequence of the axial anomaly in QCD.

The two values  $a_3$ ,  $a_8$  are well known from the hyperon decays. The SU(3) octet of axial-vector currents controls the weak  $\beta$ -decay of the neutron and spin 1/2 hyperons (e.g.  $\Lambda \rightarrow p$ ,  $\Sigma \rightarrow n$ ,  $\Xi \rightarrow \Lambda$ ). As a consequence,  $a_3$  and  $a_8$  can be expressed in terms of two parameters  $F$  and  $D$ , which are measured in the hyperon  $\beta$ -decay [126,21,32]:

$$a_3 = F + D \equiv \left| \frac{g_A}{g_V} \right| = 1.259 \pm 0.019 \quad (2.42)$$

$$a_8 = 3F - D = 0.585 \pm 0.044 \quad (2.43)$$

where  $F = 0.461 \mp 0.014$  and  $D = 0.798 \mp 0.013$ . Eq. (2.35) can be rewritten using

$$a_3 = \Delta u - \Delta d \quad (2.44)$$

$$a_8 = \Delta u + \Delta d - 2\Delta s \quad (2.45)$$

$$a_0 = \Delta u + \Delta d + \Delta s = \Delta \Sigma \quad (2.46)$$

The result is:

$$\Gamma_1^p = \frac{1}{12} a_3 + \frac{1}{36} a_8 + \frac{1}{9} a_0 \quad (2.47)$$

Thus a measurement of  $\Gamma_1$  would fix the value of  $a_0$ .

The QCD improved parton model, which will be explained in the next section, leads to corrections [37, 38] modifying Eq. (2.47) to

$$\Gamma_1^p = \frac{1}{12} \left[ (a_3 + \frac{1}{3} a_8) E_{NS}(Q^2) + \frac{4}{3} a_0 E_S(Q^2) \right] \quad (2.48)$$

with

$$E_{NS}(Q^2) = 1 - \frac{\alpha_s}{\pi} - \left( \frac{3.58}{3.25} \right) \left( \frac{\alpha_s}{\pi} \right)^2 \dots \quad (2.49)$$

$$E_S(Q^2) = 1 - \left( \frac{0.333}{0.040} \right) \frac{\alpha_s}{\pi} - \left( \frac{1.10}{-0.07} \right) \left( \frac{\alpha_s}{\pi} \right)^2 \dots \quad (2.50)$$

The upper values correspond to the number of flavours  $n_f=3$ , and the lower number to  $n_f=4$  (the result is renormalisation scheme dependent, the quoted numbers correspond to the  $\overline{MS}$  scheme).

In a first measurement of  $\Gamma_1$  and thus  $a_0$  of EMC [39, 40] the value  $\Delta \Sigma$  was compatible with zero ( $\Delta \Sigma = 0.12 \pm 0.17$ ). This value was unexpectedly small. In the naive QPM one would expect  $\Delta \Sigma = 1$ . Applying the Ellis-Jaffe sum rule leads to  $\Delta \Sigma = 0.579 \pm 0.026$  [41]. The EMC result led to the 'spin crisis in the parton model', which triggered a

(e.g. [42] - [45] and references therein). Including the new COMPASS data, shown in Fig.2.5, together with various other experiments, carried out during the last years, one can improve the accuracy of the result of  $\Delta\Sigma$  to [46]

$$\Delta\Sigma(Q^2=4(\text{GeV}/C)^2)=0.237_{-0.029}^{+0.024} \quad (2.51)$$

It establishes the small contribution of the quarks to the nucleon spin (result given in the  $\overline{MS}$  scheme). Measurements done at SMC and recently at HERMES [44] go further and allow to disentangle the contributions from the individual quark flavours to the nucleon spin. Fig.2.6 shows data from HERMES on the polarised parton distribution functions  $\Delta u(x), \Delta d(x), \Delta \bar{u}(x), \Delta \bar{d}(x)$  and  $\Delta s(x)$  .

For the neutron the first moment of  $g_1$  is

$$\Gamma_1^n = -\frac{1}{12}a_3 + \frac{1}{36}a_8 + \frac{1}{9}a_0 \quad (2.52)$$

In case of the QPM, where  $E_{NS}$  from Eq. (2.48) is unity, it follows with Eq. (2.47) that

$$\Gamma_1^p - \Gamma_1^n \equiv \frac{1}{6}a_3 = \frac{1}{6} \left| \frac{g_A}{g_V} \right| \quad (2.53)$$

Eq. (2.53) is the Bjorken sum rule, which was first derived in this form by Bjorken [49,33]. It describes a relationship between spin dependent DIS and the weak coupling constant defined in neutron  $\beta$ -decay. It only relies on the isospin invariance, i.e. on the SU(2) symmetry between up- and down-quarks. With the corrections, introduced in Eq. (2.48), it follows

$$\Gamma_1^p - \Gamma_1^n = \frac{1}{6} \left| \frac{g_A}{g_V} \right| E_{NS} \quad (2.54)$$

Beyond leading order  $E_{NS}$  depends on the number of flavours and the renormalisation scheme. Eq. (2.54) seems to be well satisfied by the data

(e.g. Ref. [51]).

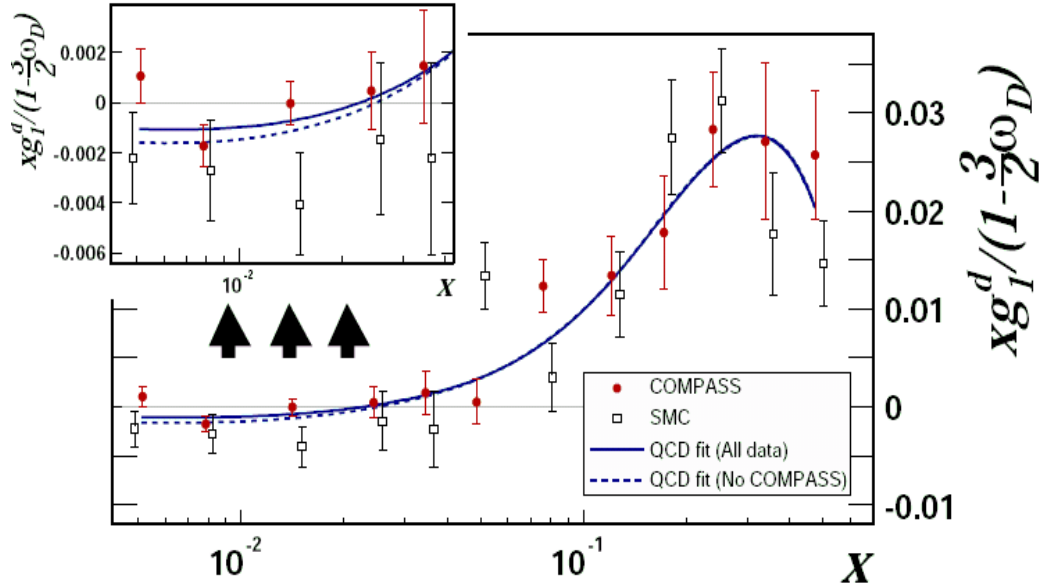


Figure 2.5: Values of  $g_1^d(x)$  measured by COMPASS (full circles) and SMC (open squares) for  $Q^2 > 1$  ( $\text{GeV}/c^2$ ). The curves represent the results of the fits at the  $Q^2$  of the COMPASS points (solid line for all data, dashed line with COMPASS excluded). The data points are corrected for the deuterium D-wave state probability  $\omega_D = 0.05$  (i.e. they correspond to the published values of  $g_1^d$  divided by 0.925).

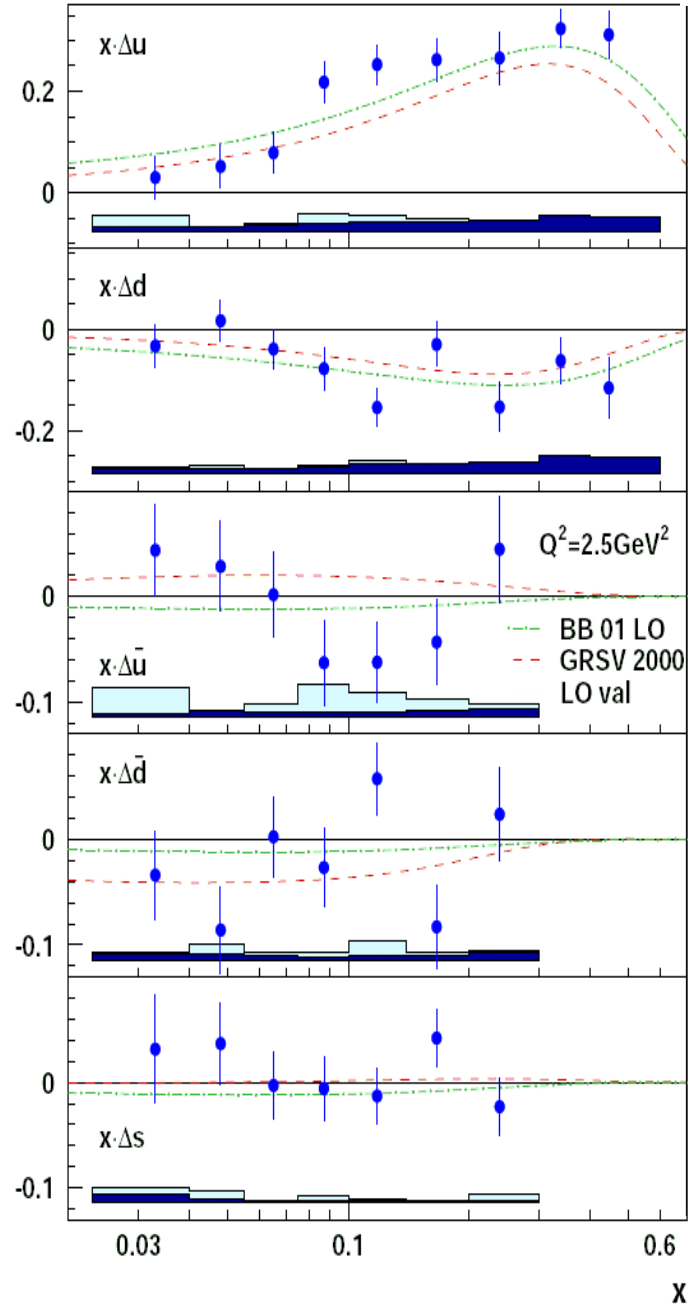


Figure 2.6: The quark helicity distributions  $x\Delta q(x, Q^2)$  evaluated at a common value of  $Q^2 = 2.5 \text{ (GeV/c)}^2$  as a function of  $x$  [44]. The dashed line is the GRSV2000 parametrization (LO, valence scenario) [47] scaled with  $1/(1+R)$  and the dashed-dotted line is the Blüemlein–Bottcher (BB) parametrization (LO, scenario 1) [48]. Figure taken from Ref. [44].

## 2.4 Improved Parton Model in QCD

### 2.4.1 Scaling Violations

Further measurements in a wider range of  $Q^2$  give a  $Q^2$ -dependence of  $F_2$ . Fig.2.7 presents measurements of  $F_2^{proton}(Q^2)$  for various values of  $x$  obtained by different experiments. This violation of Bjorken scaling is related to the gluon content inside the nucleon. Quarks can emit gluon bremsstrahlung, and gluons can split in  $q\bar{q}$  pairs and emit gluons themselves. If the quarks were not radiating gluons, exact scaling should be observed. Probing an interacting quark at a higher value of  $Q^2$ , one can resolve a gluon emission of this quark, leading to a smaller observed momentum fraction  $x$ , as illustrated in Fig. 2.8. The probability of finding a quark at lower  $x$  increases with higher  $Q^2$ , whereas finding one at high  $x$  decreases, because quarks carrying a high momentum fraction  $x$  lose momentum due to gluon radiation.

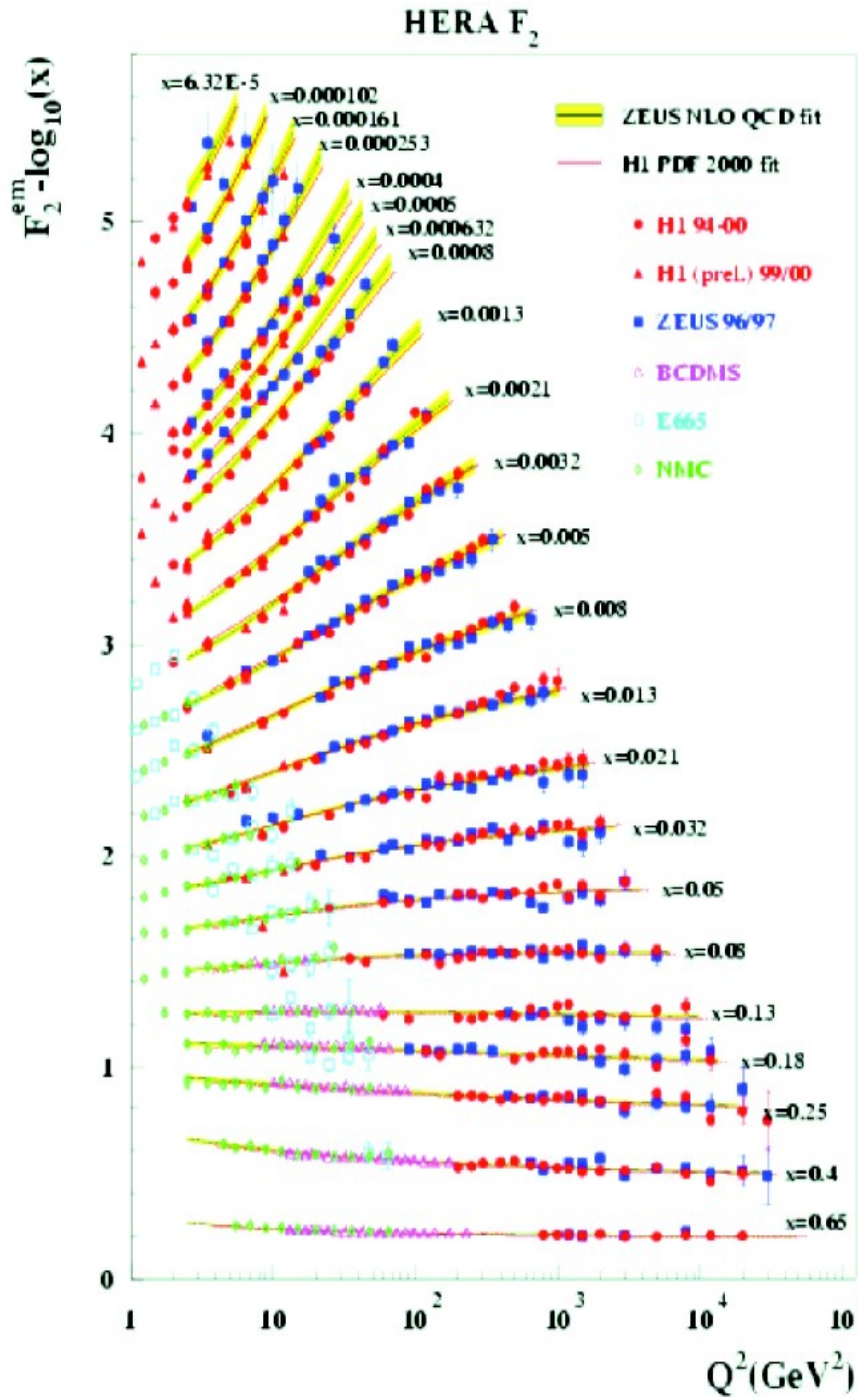


Figure 2.7: The proton structure function  $F_2(x, Q^2)$  measured in electromagnetic scattering of positrons on protons at the e-p collider HERA (ZEUS and H1).

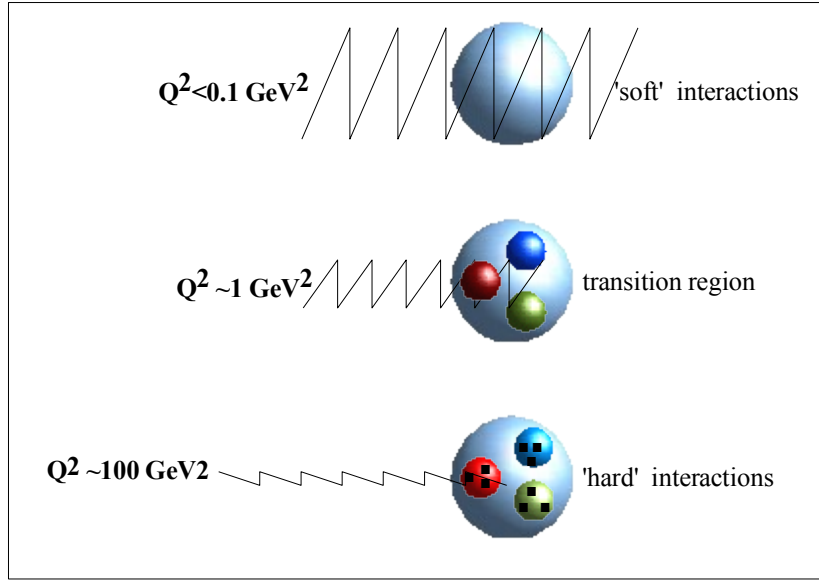


Figure 2.8. Schematic representation of photon-proton scattering for increasing photon virtuality  $Q^2$  at fixed  $W$ . As  $Q^2$  increases, the photon probes smaller transverse distance scales and is able to resolve the structure of the proton. With further increase in  $Q^2$ , quarks are resolved into more quarks and gluons.

## 2.4.2 QCD Evolution Equations

A consequence of the scaling violation is, that the quark and gluon distribution functions do not depend only on  $x$ , but also on  $Q^2$ . The  $Q^2$  dependence of the quark and gluon distributions at fixed  $x$ , but at high energy, is described by a system of coupled integro-differential equations, the DGLAP equations [52]-[54], developed by Dokshitzer, Gribov, Lipatov, Altarelli and Parisi:

$$\frac{dq^i(x, Q^2)}{d \ln Q^2} = \frac{\alpha_s(Q^2)}{2\pi} \int_x^1 \frac{dy}{y} \left[ q^i(y, Q^2) P_{qq} \left( \frac{x}{y} \right) + G(y, Q^2) P_{qG} \left( \frac{x}{y} \right) \right] \quad (2.55)$$

$$\frac{dG(x, Q^2)}{d \ln Q^2} = \frac{\alpha_s(Q^2)}{2\pi} \int_x^1 \frac{dy}{y} \left[ \sum_{i=1}^{2n_f} q^i(y, Q^2) P_{Gq} \left( \frac{x}{y} \right) + G(y, Q^2) P_{GG} \left( \frac{x}{y} \right) \right]$$

Here the running QCD coupling constant is:

$$\alpha_s(Q^2) = 4\pi / (\beta_o \ln \frac{Q^2}{\Lambda^2}) \quad \text{with} \quad \beta_o = 11 - \frac{2}{3}n_f$$

$\Lambda$  is the QCD scale parameter, and  $n_f$  the number of active quark flavours. The splitting functions  $P_{ij}$  are

$$\begin{aligned} P_{qq}(z) &= \frac{4}{3} \left( \frac{1+z^2}{1-z} \right) \\ P_{qG}(z) &= \frac{1}{2} (z^2 + (1-z)^2) \\ P_{Gq}(z) &= \frac{4}{3} \left( \frac{1+(1-z)^2}{z} \right) \\ P_{GG}(z) &= 6 \left( \frac{1-z}{z} + \frac{z}{1-z} + z(1-z) \right) \end{aligned} \tag{2.56}$$

The poles at  $z=1$  can be regularised by including virtual gluon diagrams (see Ref. [24]).  $P_{qq}$  represents the probability of a quark emitting a gluon, thus becoming a quark with a momentum fraction reduced by a fraction  $z$  (Fig. 2.9).

The DGLAP equations take into account, that a quark with momentum fraction  $x$  could have come from a parent quark with a larger momentum fraction  $y$ , which has radiated a gluon. The probability that this happens is proportional to  $\alpha_s P_{qq}(x/y)$ , when integrated over all possible momentum fractions  $y(>x)$  of the parent quark.

QCD predicts the breakdown of scaling. The value of  $q(x, Q_0^2)$  and  $G(x, Q_0^2)$  for a given  $Q^2$  allows to predict  $q(x, Q^2)$  and  $G(x, Q^2)$  at any  $Q^2$ . This so-called QCD evolution allows the determination of the gluon distribution from the measured quark distributions using the

DGLAP equations. This method has been used to determine the gluon distribution presented in Fig.2.2 in contrast to the direct measurement of  $G(x)$  in Fig.2.3. The quark distributions have to be known over a large kinematic range to achieve sufficient accuracy of the derived gluon distribution. This is the case for the unpolarised data (cf. Fig.2.7), but not for the polarised data.

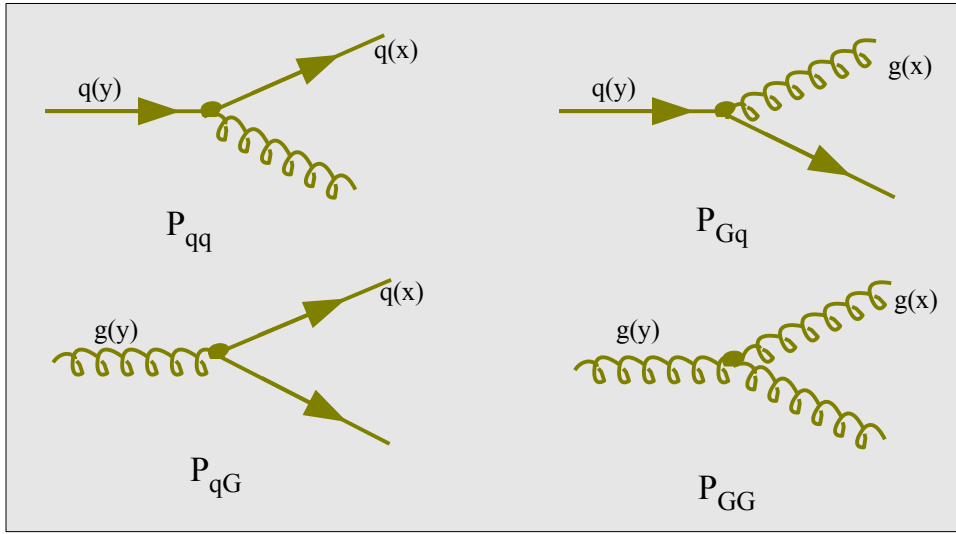


Figure 2.9: Feynman diagrams for the four splitting functions. The splitting function  $P_{ij}$  gives the probability that a parton  $i$  with momentum fraction  $x$  originates from parton  $j$ .

## QCD Evolution in the Polarised Case

The treatment of the evolution of the structure functions in the polarised case is completely analogous to the unpolarised case. It is convenient to split the polarised quark distributions into a flavour non-singlet part  $\Delta q^{NS}$  and a flavour singlet part [55]  $\Delta \Sigma$  :

$$\Delta q^{NS}(x, Q^2) = \sum_f^{n_f} \left( \frac{e_f^2}{\langle e^2 \rangle} - 1 \right) (\Delta q_f(x, Q^2) + \Delta \bar{q}_f(x, Q^2))$$

$$\Delta \Sigma(x, Q^2) = \sum_f^{n_f} \left( \Delta q_f(x, Q^2) + \Delta \bar{q}_f(x, Q^2) \right) \quad (2.57)$$

with  $\langle e^2 \rangle = \frac{1}{n_f} \sum_f e_f^2$ . The coupled DGLAP integro-differential equations for the polarised case are:

$$\frac{d}{d \ln Q^2} \Delta q^{NS}(x, Q^2) = \frac{\alpha_s}{2\pi} \Delta P_{qq}^{NS} \otimes \Delta q^{NS}(x, Q^2) \quad (2.58)$$

$$\frac{d}{d \ln Q^2} \begin{pmatrix} \Delta \Sigma(x, Q^2) \\ \Delta G(x, Q^2) \end{pmatrix} = \frac{\alpha_s}{2\pi} \begin{pmatrix} \Delta P_{qq}^S & 2n_f \Delta P_{qg}^S \\ \Delta P_{gq}^S & \Delta P_{gg}^S \end{pmatrix} \otimes \begin{pmatrix} \Delta \Sigma(x, Q^2) \\ \Delta G(x, Q^2) \end{pmatrix} \quad (2.59)$$

with the convolution

$$(P \otimes q)(x, Q^2) = \int_x^1 \frac{dy}{y} P\left(\frac{x}{y}\right) q(x, Q^2) \quad (2.60)$$

One can see that the gluons evolve like singlet combinations, i.e. sums of distribution functions. Valence quark distributions are related to non-singlet distributions, and their evolution does not depend on the gluon distribution.

The structure function  $g_1$  is given by a convolution of the singlet and non-singlet coefficient functions,  $\Delta C_S$ ,  $\Delta C_{NS}$ ,  $\Delta C_G$  with the polarised parton distribution functions

$$g_1(x, Q^2) = \frac{1}{2} \langle e^2 \rangle \left[ \Delta C_{NS} \otimes \Delta q^{NS}(x, Q^2) + \Delta C_S \otimes \Delta \Sigma(x, Q^2) + 2n_f \Delta C_G \otimes \Delta G(x, Q^2) \right] \quad (2.61)$$

The splitting and coefficient functions depend on  $x$  and  $\alpha_s(Q^2)$  and can be expanded in power series in  $\alpha_s$ :

$$\Delta C(x, \alpha_s) = \Delta C^{(0)}(x) + \frac{\alpha_s}{2\pi} \Delta C^{(1)}(x) + O(\alpha_s^2) \quad (2.62)$$

$$\Delta P(x, \alpha_s) = \Delta P^{(0)}(x) + \frac{\alpha_s}{2\pi} \Delta P^{(1)}(x) + O(\alpha_s^2) \quad (2.63)$$

At leading order (LO) one has:

$$\Delta C_S^{(0)}\left(\frac{x}{y}\right) = \Delta C_{NS}^{(0)}\left(\frac{x}{y}\right) = \delta\left(1 - \frac{x}{y}\right) \quad \text{and} \quad \Delta C_G^{(0)}\left(\frac{x}{y}\right) = 0 \quad (2.64)$$

$g_1$  decouples from  $\delta G$ , and one obtains

$$g_1(x, Q^2) = \frac{1}{2} \sum_f e_f^2 \Delta q_f(x, Q^2) \quad (2.65)$$

Here the  $x$ -dependent parton distribution functions from the quark parton model have been replaced by effective  $Q^2$  dependent distributions  $\Delta q(x, Q^2)$ .

The splitting functions in LO,  $\Delta P_{qq}^{(0)}(z) = P_{q+q+}^{(0)}(z) - P_{q-q+}^{(0)}(z)$  ( $P_{q+q+}$  corresponds to a transition from a quark  $q^+$  with positive helicity to a quark  $q^+$  with positive/negative helicity) are given by

$$\Delta P_{qq}^{(0)}(z) = P_{qq}^{(0)}(z) = C_F \left( \frac{1+z^2}{1-z} \right) \quad \text{with} \quad C_F = \frac{4}{3} \quad (2.66)$$

The polarised splitting functions are equal to the unpolarised ones, i.e.  $P_{q-q+}^{(0)}(z) = 0$ , as a consequence of helicity conservation. There is no transition between quarks of opposite helicity allowed in massless perturbative QCD (in leading order). The spin averaged splitting functions are given by the sum

$$P_{AB}^{(0)}(z) = P_{A+B+}^{(0)}(z) + P_{A-B+}^{(0)}(z) \quad (2.67)$$

The coefficient functions  $C$  and the polarised splitting functions are known to LO [52] and next-to-leading order (NLO) [56]-[58].

In leading order the gluons do not contribute to ( $\Delta C_G^{(0)} = 0$ ). But they

depend on the factorisation and renormalisation scheme in NLO. In the gauge invariant so-called Modified-Minimal-Subtraction ( $\overline{MS}$ ) scheme also the first moment of the second term in the expansion of  $\Delta C_G$  (Eq. (2.62)) vanishes. Thus  $\Delta G(x, Q^2)$  does not contribute directly to the first moment  $\Gamma_1$  of  $g_1$ . In the Adler-Bardeen (AB) scheme, which conserves chirality in contrast to  $\overline{MS}$ , the first moment of  $\Delta C_G^{(1)}$  is non-zero. Consequently  $\Gamma_1$  depends on  $\Delta G$  :

$$\Delta G(Q^2)_{\overline{MS}} = \Delta G(Q^2)_{AB} \quad (2.68)$$

$$\Delta \Sigma(Q^2)_{\overline{MS}} = a_0(Q^2) = \Delta \Sigma_{AB} - n_f \frac{\alpha_s(Q^2)}{2\pi} \Delta G(Q^2) \quad (2.69)$$

Thus the interpretation of the first moment of the structure function  $g_1(x, Q^2)$  depends on the scheme. In the  $\overline{MS}$  scheme the quark distributions depend on  $Q^2$ , in the AB-scheme they do not, but the  $Q^2$  dependence appears due to an anomalous gluon contribution explained in the next section.

Thus a small measured value of  $a_0$  does not necessarily imply that  $\Delta \Sigma$  is small, but can also be the result of the cancellation between  $\Delta \Sigma$  and the  $Q^2$  dependent gluon helicity contribution in the AB-scheme. In the  $\overline{MS}$  scheme a large gluon polarisation would be absorbed in the sea quark polarisation. Thus a large sea leads to a small measured  $a_0$ .

One way to determine  $\Delta G$  is considering the  $Q^2$  evolution of the polarised DIS data. Several groups have performed NLO fits to the polarised data. Fig.2.10 shows the results obtained by the Asymmetry Analysis Collaboration [43] compared to results from different other

groups [47] , [48], [59]-[62]. The helicity distributions for valence  $u$  and  $d$  quarks are well determined, being large and positive for  $u$  quarks and negative for  $d$  quarks. The spin carried by  $u$ -quarks is mostly parallel to the proton spin and anti-parallel for  $d$ -quarks. The sea quark helicity is small and negative with larger errors. The gluon distribution is even less well determined by the available data. This can be seen from the large errors indicated by the shaded area in Fig.2.10.

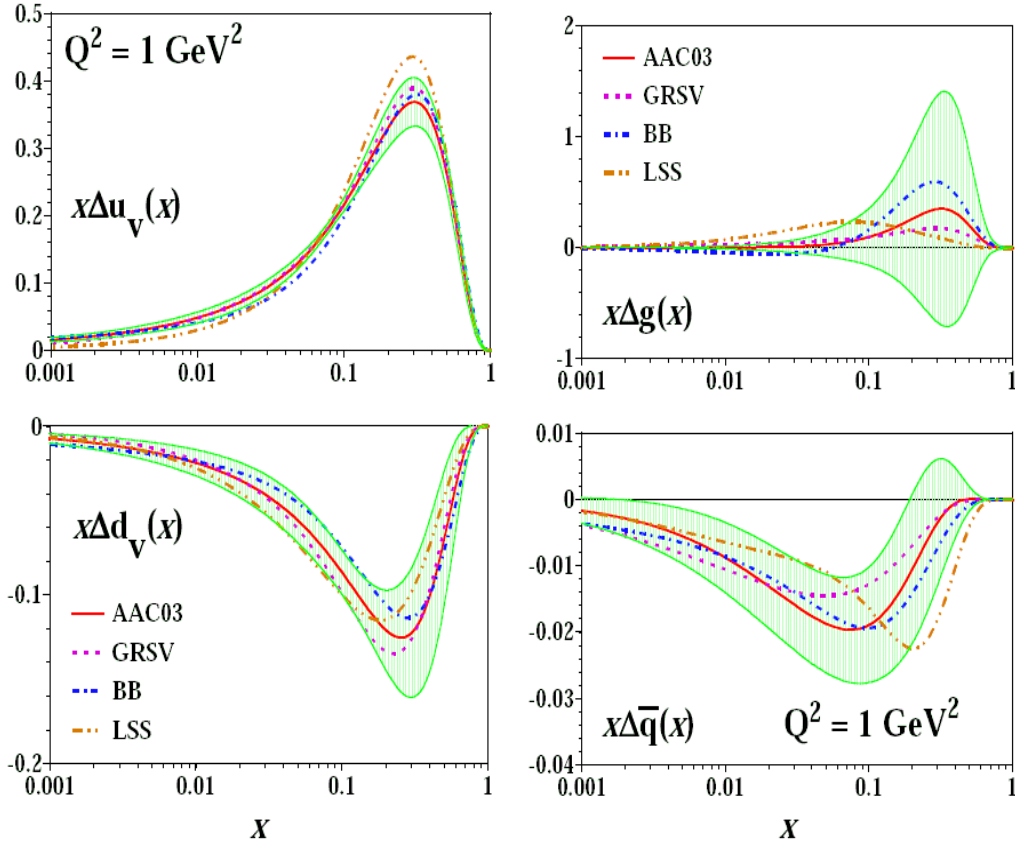


Figure 2.10: The AAC03 PDFs at  $Q^2=1\text{GeV}^2$  are compared with the ones for other parametrisations by GRSV2000 (standard scenario) [47, 59], BB (ISET=3) [48], and LSS ( $\overline{MS}$  scheme) [60, 61, 62]. The shaded areas are the uncertainties of the AAC03 analysis. Figure taken from [43].

### 2.4.3 The Axial Anomaly

The result on  $\Delta G$  can also be obtained using the operator product expansion and the already calculated proton matrix elements. Consider again the axial vector current (Eq. (2.40))

$$J_{5\mu}^f = \bar{\Psi}_f(\mathbf{x}) \gamma_\mu \gamma_5 \Psi_f(\mathbf{x})$$

made up of quark operators of a definite flavour  $f$ . From the free Dirac equation of motion one finds that

$$\partial^\mu J_{5\mu}^f = 2 i m_f \bar{\Psi}_f(\mathbf{x}) \gamma_5 \Psi_f(\mathbf{x}) \quad (2.70)$$

where  $m_f$  is the mass of the quark of flavour  $f$ . In the chiral limit,  $m_f \rightarrow 0$ , Eq. (2.70) implies that  $J_{5\mu}^f$  is conserved. However there is an anomalous contribution arising from the triangle diagram given in Fig.2.11, which leads to a non vanishing derivative in Eq. (2.70). This phenomenon has first been observed in QED by Adler [63]. In the QCD case one has [7, 8,64]

$$\partial^{5\mu} J_{5\mu}^f = \frac{\alpha_s}{4\pi} G_{\mu\nu}^a \tilde{G}_a^{\mu\nu} = \frac{\alpha_s}{2\pi} \text{Tr} [G_{\mu\nu} \tilde{G}^{\mu\nu}] \quad (2.71)$$

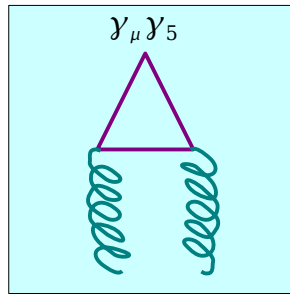


Figure 2.11: Triangle diagram giving rise to the axial anomaly. The gluons couple via the triangle to the axial current and thus contribute to the corresponding proton matrix element.

The dual gluonic field tensor  $\tilde{G}_{\mu\nu}^a$  is given by  $\tilde{G}_{\mu\nu}^a = \frac{1}{2} \epsilon_{\mu\nu\rho\sigma} G_a^{\rho\sigma}$ .

Summing over all quark flavours (here  $n_f = 3$ ), we obtain the gluonic contribution to  $a_0$ :

$$\alpha_0^{gluons}(Q^2) = -3 \frac{\alpha_s}{2\pi} \Delta G(Q^2) \quad (2.72)$$

The anomaly introduces a pointlike interaction between the axial vector current and the gluons, because it does not depend on the momentum transfer  $k_1 - k_2$  when  $m_f = 0$ , where  $k_1$  and  $k_2$  are the gluon momenta in Fig.2.11. Therefore one obtains a contribution to the matrix element of a hadron state from the gluonic component of the hadrons as well as from the quarks [19]. Eq. (2.72) is believed to be an exact result and not to be affected by higher order corrections [66].

As a consequence of Eq. (2.72)  $a_0$  has contributions from quarks and gluons. In the AB scheme we obtain the result for  $a_0$  given in Eq.(2.69):

$$\alpha_0(Q^2) = \Delta \Sigma - 3 \frac{\alpha_s}{2\pi} \Delta G(Q^2) \quad (2.73)$$

The gluonic term in Eq. (2.73) does not vanish at large  $Q^2$ , since the gluon spin behaves just as  $[\alpha_s(Q^2)]^{-1}$  for  $Q^2 \rightarrow 0$  [64,67]. In the gauge invariant  $\overline{MS}$  scheme the term containing  $\Delta G$  in Eq. (2.73) is cancelled by an additional term, and there is no anomaly.

## 2.5 Fragmentation

Thus far only inclusive DIS experiments, in which the incoming and the scattered lepton are measured, were discussed quantitatively. Detecting a hadron in coincidence with the scattered lepton is intimately related to the initial quarks and thus provides important information on the nucleon structure. Fig.2.12 illustrates the process, which is similar to the inclusive lepton-nucleon scattering plus one extra degree of freedom,

associated with the momentum  $p_h$  of the additionally detected hadron. The additional variable, used to describe this process, is the energy fraction of the virtual photon energy carried by the hadron

$$z = \frac{E_h}{\nu} \quad (2.74)$$

Alternatively one can use the Feynman variable:

$$x_F = \frac{p_z^{c.m.}}{p_{z,max}^{c.m.}} \approx \frac{2 p_z^{c.m.}}{W}, \quad (2.75)$$

( $p_z$ : longitudinal momentum fraction in the photon-nucleon c.m. system).

The region of  $x_f < 0$  selects preferably hadrons from the target fragmentation region, which originate from the target remnant. Hadrons, which originate from the struck quark, are produced in the current fragmentation region.

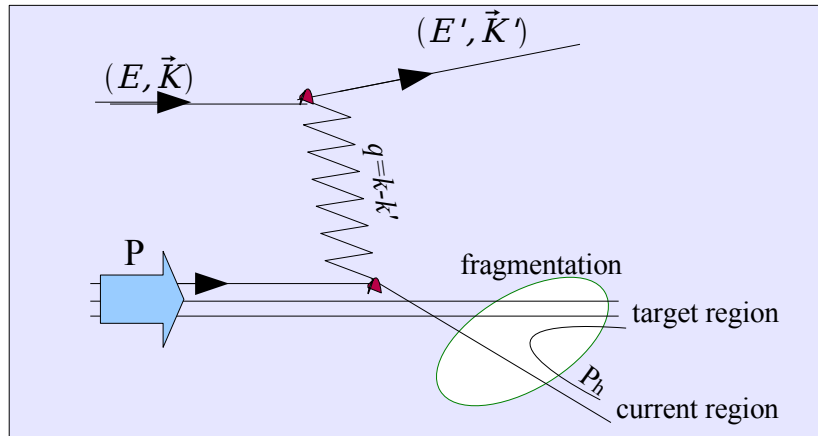


Figure 2.12: Schematic representation of hadron production in DIS.

The formation of hadrons is due to the confinement property of QCD, which demands that only neutral colour objects exist as free particles.

Thus the struck quark and the target remnant have to form colour neutral final state hadrons. This process of hadronisation cannot be described by perturbative QCD, but it is parametrised by the fragmentation functions. It is assumed, that the factorisation of the hard process and the fragmentation process holds. Thus the hard process can be calculated, using perturbative QCD, and the soft part, (the fragmentation) is parametrised independently. This is in analogy to the treatment of the inclusive cross section. The hard process is independent of the parton distributions, which are the non-perturbative soft part. The cross section is a product of both.

The current region allows to obtain information about the struck quark. The charge, the identity and the direction of the leading hadron is correlated to the flavour and the direction of the struck quark. The cross section for the production of a particular hadron  $h$  can be written, in leading order QCD, as

$$\sigma^h(x, Q^2, z) \propto \sum_f e_f^2 q_f(x, Q^2) D_f^h(z, Q^2) \quad (2.76)$$

where  $D_f^h(z, Q^2)$  is the fragmentation function parametrising the fragmentation process. The fragmentation function gives the probability density that a struck quark of flavour  $f$ , probed at a scale  $Q^2$ , fragments into a hadron  $h$  of energy  $E_h$  being a fraction  $z$  of the virtual photon energy. The fragmentation functions are normalised to the particle multiplicities and conserve energy:

$$\sum_h \int_0^1 z D_f^h(z, Q^2) dz = 1 \quad (2.77)$$

Isospin symmetry and charge conjugation limits the number of independent  $D_q^h(z)$ , e.g. for a pion,

$$D_u^{\pi^+} = D_d^{\pi^-} = D_{\bar{d}}^{\pi^+} = D_{\bar{u}}^{\pi^-} \quad (2.78)$$

$$D_d^{\pi^+} = D_u^{\pi^-} = D_{\bar{u}}^{\pi^+} = D_{\bar{d}}^{\pi^-} \quad (2.79)$$

$$D_s^{\pi^+} = D_s^{\pi^-} = D_{\bar{s}}^{\pi^+} = D_{\bar{s}}^{\pi^-} \quad (2.80)$$

The  $D_u^{\pi^+}$  etc. are the so-called favoured fragmentation functions,  $D_d^{\pi^+}$  the unfavoured fragmentation functions, and  $D_s^{\pi^+}$  the strange fragmentation function. For the favoured fragmentation the initial quark is in the pion ground state wavefunction, and such processes are more probable than the unfavoured or strange cases.

Thus one can draw conclusions about the struck quark when identifying the leading hadron in an experiment. This allows e.g. a flavour separated determination of the (polarised) parton distributions as shown in Fig.2.2 and 2.6.

## CHAPTER 3

### The Gluon Helicity Distribution $\Delta G(x, Q^2)$

The gluon contribution to the spin of the nucleon can be separated into spin and orbital parts. As with its unpolarized counterpart, the polarized gluon distribution is difficult to access experimentally. There exists no hard scattering process, which would allow to measure this distribution. In a longitudinally-polarized nucleon the polarized gluon distribution  $\Delta G(x, Q^2)$  contributes to the spin-dependent scattering processes. In QCD, using the infrared factorization of a hard process,  $\Delta G(x, Q^2)$  can be calculated as a matrix element of the non-local operator[50]

$$\Delta G(x, Q^2) = \frac{-i}{x} \int \frac{d\lambda}{2\pi} e^{-i\lambda x} \langle P | F^{+\alpha}(\lambda n) W \tilde{F}_\alpha^+(0) | P \rangle \quad (3.1)$$

where  $|P\rangle$  is the proton state normalized covariantly,  $n$  is a light-like vector conjugating to an infinite momentum frame  $P$ .  $\tilde{F}_{\alpha\beta} = \frac{1}{2} \epsilon_{\alpha\beta\mu\nu} F^{\mu\nu}$  is the gluon field tensor and  $W$  is a gauge link along the direction  $n$  connecting the two gluon field tensors, making the operator gauge invariant. Because of the charge conjugation property of this operator, the gluon distribution is symmetric in  $x$ :

$$\Delta G(x, Q^2) = \Delta G(-x, Q^2) \quad .$$

The even moments of  $\Delta G(x, Q^2)$  are directly related to the matrix elements of local operators. Defining

$$\int_{-1}^1 dx x^{n-1} \Delta G(x, Q^2) = a_n(\mu^2) \quad , \quad (n=1,3,5\dots) \quad (3.2)$$

we find

$$\langle P | F^{\mu_1 \alpha} iD^{\mu_2} \dots iD^{\mu_{n-1}} i \tilde{F}_{\alpha}^{\mu_n} | P \rangle = 2a_n(\mu^2) S^{\mu_1} P^{\mu_2} \dots P^{\mu_n} \quad (3.3)$$

The renormalization scale dependence is directly connected to the renormalization of the local operators. Because Eq. (3.1) involves directly the time variable, it is difficult to evaluate the distribution on a lattice. The matrix elements of local operators can be calculated in lattice QCD. Hence the moments of  $\Delta G(x, Q^2)$  are, in principle, calculable.

From these equations it is clear that the first-moment ( $n=1$ ) of  $\Delta G(x)$  does not correspond to a gauge-invariant local operator. In the axial gauge  $n \cdot A = 0$  the first moment of the nonlocal operator can be reduced to a local one,  $\vec{E} \times \vec{A}$ , which can be interpreted as the gluon spin density operator. The first moment of  $\Delta G(x, \mu^2)$  represents the gluon spin contribution to the nucleon spin in the axial gauge. In any other gauge it cannot be interpreted in this way. One can formally write  $J_g = \Delta G + L_g$  in the axial gauge, where  $L_g$  is the gluonic orbital contribution to the nucleon spin. There is no way to measure  $L_g$  directly in the experiments.

### 3.1 Next-to-Leading Order Evolution of $g_1(x, Q^2)$

The spin structure functions possess a significant  $Q^2$  dependence due to the QCD radiative effects. It is important to understand these effects. As the experiments are carried out at different accelerator facilities with different beam energies, the data cover a range of  $Q^2$ . In addition, due to the extensive data set that has been accumulated and the recently computed higher-order QCD corrections, it is possible to produce parameterizations based on Next-to-Leading-Order (NLO) QCD fits to the data. This provides an important input to future experiments utilizing

polarized beams (e.g., the RHIC spin program). These fits have also given information on the gluon spin distribution, due to the radiative effects that couple the quark and gluon spin distributions at NLO.

At NLO the spin structure function becomes

$$g_1(x, Q^2) = \frac{1}{2} \sum_i e_i^2 C_q(x, \alpha_s) \otimes \Delta q_i(x, Q^2) + \frac{1}{N_f} C_g(x, \alpha_s) \otimes \Delta G(x, Q^2) \quad (3.4)$$

where the sum is again over the quarks and antiquarks:  $u, d, s, \bar{u}, \bar{d}, \bar{s}$ .  $C_q(x, \alpha_s)$  and  $C_g(x, \alpha_s)$  are Wilson coefficients and correspond to the polarized photon-quark and photon-gluon hard scattering cross section respectively. The convolution  $\otimes$  is defined as

$$C(x, \alpha_s) \otimes q(x, Q^2) = \int_x^1 \frac{dy}{y} C\left(\frac{x}{y}, \alpha_s\right) q(y, Q^2) \quad (3.5)$$

The explicit dependence of the nucleon spin structure function on the gluon spin distribution is apparent in Eq. (3.4). At Leading Order (LO) one has  $C_q^0 = \delta(1-x)$  and  $C_g^0 = 0$ , and the usual dependence (Eq.(3.4)) of the spin structure function on the quark spin distributions emerges. At NLO the factorization between the quark spin distributions and coefficient functions shown in Eq.(3.4) cannot be defined unambiguously. This is known as factorization scheme dependence and results from an ambiguity in the division between the definition of the quark/gluon spin distributions and the coefficient functions. There are also ambiguities associated with the definition of the  $\gamma_5$  matrix in  $n$  dimensions [77] and with the inclusion of the axial anomaly. This has lead to a variety of factorization schemes that deal with these ambiguities.

We can classify the factorization schemes in terms of their treatment

of the higher order terms in the expansion of the coefficient functions. The  $Q^2$  dependence of this expansion can be written as:

$$C_i(x, \alpha_s) = C_i^0(x) + \frac{\alpha_s(Q^2)}{2\pi} C_i^{(1)} + \dots \quad (3.6)$$

In the so-called Modified-Minimal-Subtraction ( $\overline{MS}$ ) scheme [78,79] the first moment of the NLO correction to  $C_g$  vanishes (i.e.

$$\int_0^1 C_g^{(1)}(x) dx = 0). \text{ Thus } \Delta G \text{ does not contribute to the first moment of}$$

$g_1$ . In the Adler-Bardeen [80,81] scheme (AB) the treatment of the axial anomaly causes the first moment of  $C_g^{(1)}$  to be non-zero, leading to a dependence of  $\int g_1(x) dx$  on  $\int \Delta G(x) dx$ . This leads to a difference in the singlet quark distribution in the two schemes:

$$\Delta \Sigma(x, Q^2)_{AB} = \Delta \Sigma(x, Q^2)_{\overline{MS}} + N_f \frac{\alpha_s(Q^2)}{2\pi} \int_x^1 \frac{dy}{y} \Delta G(y, Q^2) \quad (3.7)$$

$$\Delta G(x, Q^2)_{AB} = \Delta G(x, Q^2)_{\overline{MS}}$$

A third scheme, sometimes called the JET scheme [82,83] or chirally invariant (CI) scheme [84], is also used. This scheme attempts to include all perturbative anomaly effects into  $C_g$ . Of course, physical observables (eg.  $g_1(x, Q^2)$ ) are independent of the choice of the scheme. There are also straightforward transformations [81,85,86] that relate the schemes and their results to one another.

Once a choice of scheme is made, the  $Q^2$  dependence of  $g_1$  can be calculated using the (*DGLAP*) equations[87]. These equations characterize the evolution of the spin distributions in terms of  $Q^2$  dependent splitting functions  $P_{ij}(x, \alpha_s)$ :

$$\frac{d}{d \ln(Q^2)} \Delta q_{NS}(x, Q^2) = \frac{\alpha_s(Q^2)}{2\pi} P_{qq}^{NS} \otimes \Delta q_{NS} \quad (3.8)$$

$$\frac{d}{d \ln(Q^2)} \begin{pmatrix} \Delta \Sigma \\ \Delta G \end{pmatrix} = \frac{\alpha_s(Q^2)}{2\pi} \begin{pmatrix} P_{qq} & P_{qg} \\ P_{gq} & P_{gg} \end{pmatrix} \otimes \begin{pmatrix} \Delta \Sigma \\ \Delta G \end{pmatrix}$$

The non-singlet quark distributions  $\Delta q_{NS}(x, Q^2)$  for three quark flavors are defined as

$$\Delta q_{NS}(x, Q^2) = (\Delta u + \Delta \bar{u}) - \frac{1}{2}(\Delta d + \Delta \bar{d}) - \frac{1}{2}(\Delta s + \Delta \bar{s}) \quad (3.9)$$

The splitting functions  $P_{ij}$  can be expanded in a form similar to that for the coefficient functions  $C_i(x, \alpha_s)$  in Eq.(3.6) and have been recently evaluated [78,79] in NLO.

The remaining ingredients are the choice of the starting momentum scale  $Q_0^2$  and the form of the distributions at this  $Q_0^2$ . The momentum scale is usually chosen to be  $\leq 1 \text{ GeV}^2$ . Thus the quark spin distributions are dominated by the valence quarks. The gluon spin distribution is likely to be small. Also, as discussed above, at lower momentum transfer some models for the  $x$  dependence of the distributions (eg. Regge-type models for the low  $x$  region) are more reliable. The form of the polarized parton distributions at the starting momentum scale are parameterized by a variety of  $x$  dependences with various powers. This parameterization is the source of large uncertainties, as the  $x$  dependence at low values of  $x \leq 0.003$  is largely unconstrained by the measurements. An example: in ref[81] it is assumed, that the polarized parton distributions can be parameterized by

$$\Delta q_i(x, Q_0^2) = A_i x^{\alpha_i} (1-x)^{\beta_i} (1+\gamma_i x^{\delta_i}) \quad (3.10)$$

With such a large number of parameters it is usually required to place

additional constraints on some of the parameters. Often  $SU(3)_f$  symmetry is used to constrain the parameters, or the positivity of the distributions ( $|\Delta q_i(x)| \leq q_i(x)$ ) is enforced (note that this positivity is strictly valid only when all orders are included; see Ref. [88]). In other fits the polarized distributions are taken to be proportional to the unpolarized distributions (as in Ref. [75]):

$$\Delta q_i(x, Q_0^2) = A_i x^{\alpha_i} q_i(x, Q_0^2) \quad (3.11)$$

A large number of NLO fits have recently been published [75,80,81,86,89-98]. These fits include a wide variety of assumptions for the forms of the polarized parton distributions, differences in the factorization scheme and the selection of data sets included in the fit (only the most recent fits [97] include all the published inclusive data). Some fits [98] have even performed a NLO analysis including information from semi-inclusive scattering. A comparison of the results from some of these recent fits is shown in Table (3.1).

Note that in the JET and AB schemes  $\Delta \Sigma$  includes a contribution from  $\Delta G$ . Thus the result of these fits is that the quark spin distribution  $\Delta \Sigma$  is constrained between 0.05 – 0.30. However the gluon distribution and its first moment are largely unconstrained. The extracted value for  $\Delta G(Q^2=5 \text{ GeV}^2)$  is typically positive, but the corresponding uncertainty is often 50–100%. Note that the uncertainties listed in Table (3.1) are dependent on the assumptions used in the fits.

Estimates of the contribution from higher twist effects [103,104] ( $1/Q^2$  corrections) suggest that the effects are relatively small at the present experimental values of  $Q^2$ . This is further supported by the fits that the NLO QCD calculations can achieve, without including possible higher-twist effects.

Lattice QCD calculations of the first and second moments of the polarized spin distributions are carried out [99-102]. The agreement with NLO fits to the data is reasonable for the quark contribution, although the lattice calculations are not yet able to calculate the gluon contribution.

Table (3.1): Results from NLO fits to data for first moments of quark and gluon distributions. Missing data refers to data sets that are not included in the fits, pPDF refers to the assumptions for Polarized Distribution Functions, and  $Q_{ev}^2$  refers to the evolved  $Q^2$  where the first moments are evaluated.

Reference	Scheme	$Q_0^2$ GeV <sup>2</sup>	Missing Data	pPDF	$Q_{ev}^2$ GeV <sup>2</sup>	$\Delta \Sigma$	$\Delta G$
ABFR98[81] (Fit-A)	AB	1	HERMES(p) E155(pd) Semi-inc	$\Delta q_i \propto q_i$	1	0.41±0.03	0.95±0.18
LSS99 [96]	JET	1	Semi-inc	$\Delta q_i \propto q_i$	1	0.39±0.04	0.57±0.14
	AB	1				0.41±0.04	0.58±0.04
	$\overline{MS}$	1				0.28±0.04	0.07±0.10
GOTO00[97] (NLO-1)	$\overline{MS}$	1	Semi-inc	$\Delta q_i \propto q_i$	1	0.050	0.53
		1			5	0.054	0.86
		1			10	0.055	1.0
FS00 [98] (ii)	$\overline{MS}$	0.5	–	$\Delta q_i \propto q_i$	10	0.050	0.53

### 3.2 Gluon helicity distribution from the QCD Scale Evolution

The polarized gluon distribution enters in the factorization formula for spin-dependent inclusive deep-inelastic scattering. Since the structure function  $g_1(x, Q^2)$  involves both the singlet quark and gluon distributions, as shown in Eq.(3.4), only the  $Q^2$  dependence of the data can be exploited to separate them. The  $Q^2$  dependence results from two different sources: the running coupling  $\alpha_s(Q^2)$  in the coefficient

functions and the scale evolution of the parton distributions. As the gluon contribution has its own characteristic  $Q^2$  behavior, it can be isolated in principle from the data taken over a wide range of  $Q^2$ .

Because the currently available experimental data have rather limited  $Q^2$  coverage, there is at present a large uncertainty in extracting the polarized gluon distribution. A number of NLO fits have been performed to extract the polarized parton densities. While the results for the polarized quark densities are relatively stable, the extracted polarized gluon distribution depends strongly on the assumptions made about the  $x$ -dependence of the initial parameterization. Different fits produce results at fixed  $x$  differing by an order of magnitude. Even the sign is not well constrained.

Several sets of polarized gluon distributions have been used in the literature for the purpose of estimating the results of the future experiments. The range of possible distributions is shown in Fig. (3.1) (Ref.[90]). The real gluon distribution could be very different from the ones shown.

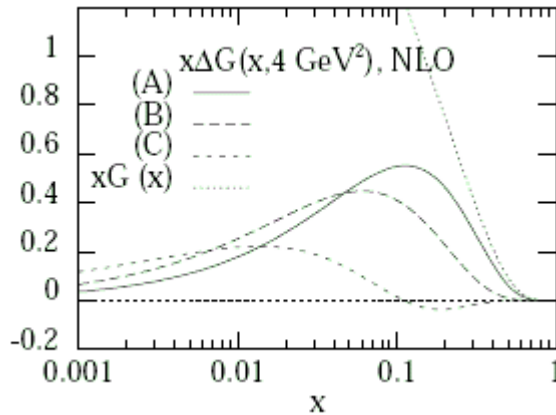


Figure (3.1): Typical gluon helicity distributions [90] obtained from fits to the available polarized DIS data.

### 3.3 Gluon helicity distribution from Di-jet Production in $e-p$ Scattering

In deep-inelastic scattering the virtual photon can generate two jets with large transverse momenta. To leading-order in  $\alpha_s$ , the underlying hard scattering subprocesses are Photon-Gluon Fusion (PGF) and QCD Compton Scattering (QCDC) (see Fig. (3.2)). If the initial photon has momentum  $q$  and the quark or gluon from the nucleon (with momentum  $P$ ) has momentum  $xp$ , the invariant mass of the di-jet is  $\hat{s}=(q+xp)^2$ . The  $x$ -parameter, at which the densities are probed is given by:

$$xp = x_B \left( \frac{1 + \hat{s}}{Q^2} \right) \quad (3.12)$$

where  $x_B$  is the Bjorken  $x$  variable. The di-jet invariant mass fixes the momentum fraction. Depending on the relative sizes of  $\hat{s}$  and  $Q^2$ ,  $x$  can be an order of magnitude larger than  $x_B$ .

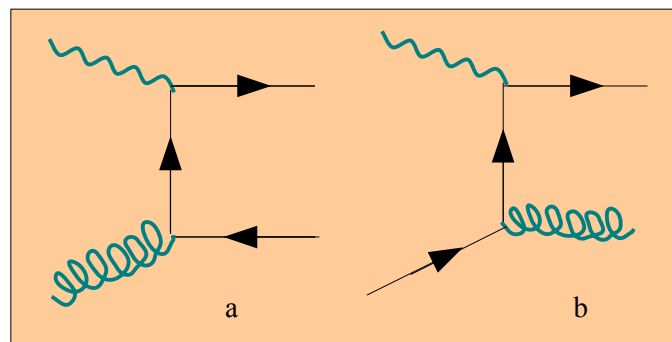


Figure (3.2): Leading-order Feynman diagrams for di-jet production in DIS: (a) Photon-Gluon Fusion, (b) Photon-Quark Compton scattering.

If the contribution from the quark initiated subprocess is small, or the quark distribution is known, the two-jet production is a useful process to measure the gluon distribution. The di-jet invariant mass provides direct

control over the fraction of the nucleon momentum carried by the gluon ( $x_G = xp$ ). The di-jet data from *HERA* have been used by the *H1* and *ZEUS* collaborations to extract the unpolarized gluon distribution [105, 106]. With a polarized beam and target, the process is ideal for probing the polarized gluon distribution.

The unpolarized di-jet cross section for photon-nucleon collisions can be written as [107]

$$\sigma_{di-jet}(q, xp) = \sigma_{di-jet}^{PGF} + \sigma_{di-jet}^{QDC} = AG(x) + Bq(x) \quad (3.13)$$

where  $G(x)$  and  $q(x)$  are the gluon and quark densities, respectively, and  $A$  and  $B$  are the hard scattering cross sections calculable in perturbative QCD (pQCD). Similarly, the polarized cross section can be written as

$$\Delta\sigma_{dj-jet}(q, xp) = \sigma_{dj-jet}^{++} - \sigma_{dj-jet}^{+-} = a\Delta G(x) + b\Delta q(x) \quad (3.14)$$

where the first and second (+, -) refer to the helicities of the photon and nucleon, respectively. The double spin asymmetry for di-jet production is given by:

$$A_{di-jet} = \frac{\Delta\sigma_{di-jet}}{2\sigma_{di-jet}} = \frac{a}{A} \frac{\Delta G(x)}{G(x)} \frac{\sigma_{di-jet}^{PGF}}{2\sigma_{di-jet}} + \frac{b}{B} \frac{\Delta q(x)}{q(x)} \frac{1}{2} \left( 1 - \frac{\sigma_{di-jet}^{PGF}}{\sigma_{di-jet}} \right) \quad (3.15)$$

The experimental asymmetry  $A_{exp}$  in DIS is related to the photon asymmetry by

$$A_{exp} = P_e P_N D A_1^{di-jet} \quad (3.16)$$

where  $P_e$  and  $P_N$  are the electron and nucleon polarizations, respectively, and  $D$  is the depolarization factor of the photon.

At low  $x$  the gluon density dominates over the quark density. Thus the photon-gluon fusion subprocess dominates, and we have

$$A_1^{di-jet} = \frac{a}{A} \frac{\Delta G(x)}{2G(x)} \quad (3.17)$$

This provides a direct measurement of the gluon polarization. Due to the helicity selection rule the photon and gluon must have opposite helicities to produce a quark and antiquark pair, and hence  $a/A = -1$ . Therefore, if  $G(x)$  is positive, the spin asymmetry must be negative. Leading-order calculations in Refs. [107-110] show, that the asymmetry can be exploited if it is large and depends on the gluon polarization.

At NLO the one-loop corrections for the PGF and QCDC subprocesses must be taken into account. Three-jet events with two of the jets too close to be resolved, must be treated as two-jet production. The sum of the virtual ( $2 \rightarrow 2$  processes with one loop) and real ( $2 \rightarrow 3$  leading-order processes) corrections are independent of the infrared divergence. The two-jet cross section depends on the scheme in which the jets are defined. NLO calculations, carried out in Refs. [111-113], show that the strong sensitivity of the cross section to the polarized gluon distribution survives. In terms of the spin asymmetry, the NLO effects do not significantly change the result.

Since the invariant mass of the di-jet is itself a large mass scale, two-jet production can also be used to measure  $\Delta G(x)$ , even when the virtuality of the photon is small or zero (real photon). A great advantage of using nearly real photons is, that the cross section is large due to the infrared enhancement, and hence the statistics is high. A disadvantage is, that there is now a contribution from the resolved photons. Because the photon is nearly on-shell, it has a complicated hadronic structure of its own. The structure can be described by quark and gluon distributions, which have not yet been well determined experimentally. Some models of the spin-dependent parton distributions in the photon are discussed in Ref. [114]. Leading-order calculations [115,116] show, that there are

kinematic regions, in which the resolved photon contribution is small, and the experimental di-jet asymmetry can be used favorably to constrain the polarized gluon distribution.

### **3.4 Gluon helicity distribution from Large- $p_T$ Hadron Production in e-p Scattering**

For e-p scattering at moderate center-of-mass energies, as in fixed target experiments, jets are hard to identify because of their large angular spread and the low hadron multiplicity. However one still expects that the leading hadrons in the final state reflect to a certain degree the original parton directions and flavors (discounting the transverse momentum, of order  $\Lambda(QCD)$ , from the parton intrinsic motion in hadrons and from their fragmentation). If so, one can try to use the leading high- $p_T$  hadrons to tag the partons produced in the hard subprocesses considered in the previous subsection.

Bravar et al. [117] have proposed to use high- $p_T$  hadrons to gain access to  $\Delta G(x)$ . To enhance the relative contribution from the photon-gluon fusion subprocess and hence the sensitivity of physical observables to the gluon distribution, they propose a number of selection criteria for the analysis of the data and then test these criteria in a Monte Carlo simulation of the COMPASS experiment. These simulations show that these cuts are effective in selecting the gluon-induced subprocess. Moreover, the spin asymmetry for the two-hadron production is large (10-20%) and is strongly sensitive to the gluon polarization.

Because of the large invariant mass of the hadron pairs, the underlying subprocesses can still be described in perturbative QCD, even if the virtuality of the photon is small or zero [118]. This enhances the data

sample, but introduces additional sub-processes to the high- $p_T$  hadron production. The contribution from the resolved photons, eg. from  $\gamma \rightarrow \bar{q}q$  fluctuations, appears not to overwhelm the PGF contribution. Photons can also fluctuate into  $\rho$  mesons. The  $\rho$ -nucleon scattering produces large- $p_T$  hadron pairs. The experimental information on this process can be used to subtract its contribution. After taking into account these contributions, it appears that the photons of low virtuality can be used as an effective probe of the gluon distribution to complement the data from DIS lepton scattering.

### 3.5 Gluon helicity distribution from open-charm (heavy-quark) production in e-p Scattering

Heavy quarks can be produced in e-p scattering through photon-gluon fusion and can be calculated in pQCD (see Fig. (3.3)). In the deep-inelastic scattering region, the charm quark contribution to the  $g_1(x, Q^2)$  structure function is known [119],

$$g_1^c(x, Q^2) = \frac{\alpha_s(\mu^2)}{9\pi} \int_{ax}^1 \frac{dy}{y} \Delta P\left(\frac{x}{y}, Q^2\right) \Delta G(y, \mu^2) \quad (3.18)$$

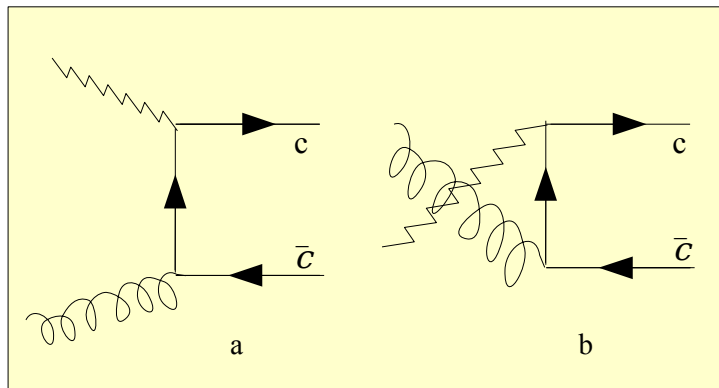


Figure (3.3): Feynman diagrams for charm production via Photon Gluon Fusion.

where  $a=1+\frac{4m_c^2}{Q^2}$  and

$$\Delta P(x, Q^2) = (2x-1) \ln \frac{1+\eta}{1-\eta} + \eta(3-4x) \quad (3.19)$$

with  $\eta^2 = 1 - \frac{4m_c^2}{Q^2(1-x)}$ . This result assumes that due to the large charm quark mass the direct charm contribution (eg. through  $\Delta c(x)$ ) is small and the light-quark fragmentation production of charm mesons is suppressed. The  $x$  dependence of the structure function, if measured, can be deconvoluted to give the polarized gluon distribution. The renormalization scale  $\mu$  can be taken to be twice the charm quark mass  $2m_c$ .

Following Ref. [120], the open charm electro-production cross section is large when  $Q^2$  is small or vanishes. It can be written as follows:

$$\frac{d^2 \sigma^{\mu N \rightarrow c \bar{c} x}}{dQ^2 d\nu} = \Gamma(E; Q^2, \nu) \sigma^{\gamma^* N \rightarrow c \bar{c} x}(Q^2, \nu) \quad (3.20)$$

Here the virtual photon flux is

$$\Gamma(E; Q^2, \nu) = \frac{\alpha_{em}}{2\pi} \frac{2(1-y) + y^2 + Q^2/2E^2}{Q^2(Q^2 + \nu^2)^{1/2}} \quad (3.21)$$

( $E$  and  $\nu$  are the lepton and photon energies and  $y = \nu/E$ ).

For a fixed  $y$ , the flux is inversely proportional to  $Q^2$ . The second factor in Eq.(3.20) is the photonucleon cross section.

The cross section asymmetry is simple for  $Q^2=0$ . The total parton cross section for photon-gluon fusion is

$$\sigma(\hat{s}) = \frac{8\pi\alpha_{em}\alpha_s(\hat{s})}{9\hat{s}} \left[ -\beta(2-\beta^2) + \frac{1}{2}(3-\beta^4) \ln \frac{1+\beta}{1-\beta} \right] \quad (3.22)$$

where  $\beta = \sqrt{1 - 4m_c^2/\hat{s}}$  is the center-of-mass velocity of the charm quark, and  $\hat{s} = (q + x_G P)^2$  is the invariant mass of the photon-gluon system. On

the other hand, the spin-dependent cross section is

$$\Delta\sigma = \frac{8\pi\alpha_{em}\alpha_s(\hat{s})}{9\hat{s}} \left[ 3\beta - \ln \frac{1+\beta}{1-\beta} \right] \quad (3.23)$$

The photon-nucleon asymmetry for open charm production can be obtained by convoluting the above cross sections with the gluon distribution, giving

$$A_{yN}^{c\bar{c}}(E, y) = \frac{\Delta\sigma^{yN \rightarrow c\bar{c}x}}{\sigma^{yN \rightarrow c\bar{c}x}} = \frac{\int_{4m_c^2}^{2ME_y} d\hat{s} \Delta\hat{\sigma}(\hat{s}) \Delta G(x_G, \hat{s})}{\int_{4m_c^2}^{2ME_y} d\hat{s} \hat{\sigma}(\hat{s}) G(x_G, \hat{s})} \quad (3.24)$$

where  $x_G = \frac{\hat{s}}{2M_N Ey}$  is the gluon momentum fraction. Ignoring the  $Q^2$  dependence, the  $l$ - $P$  spin asymmetry is related to the photon-nucleon spin asymmetry by  $A_{lN}^{c\bar{c}} = D A_{yN}^{c\bar{c}}$ , where  $D$  is the depolarization factor introduced before.

The NLO corrections have recently been calculated by Bojak and Stratmann [121] and Contogouris et al. [122]. The scale uncertainty is considerably reduced in NLO, but the dependence on the precise value of the charm quark mass is sizable at fixed target energies.

Besides the total charm cross section one can study the distributions of the cross section in the transverse momentum or rapidity of the charm quark. The benefit of doing this is that one can avoid the region of small  $x_G$ , where the asymmetry is very small [115].

Open charm production can be measured by detecting  $D^0$  mesons from charm quark fragmentation. On average, a charm quark has about 60% probability of fragmenting into a  $D^0$ . The  $D^0$  meson can be reconstructed through its two-body decay mode  $D^0 \rightarrow K^- + \pi^+$ ; the

branching ratio is about 4%. Additional background reduction can be achieved by tagging  $D^{*+} \rightarrow D^0 \pi^+$  through detection of the additional  $\pi^+$ .

$J/\psi$  production is, in principle, also sensitive to the gluon densities. However, because of ambiguities in the production mechanisms [123], any information on  $\Delta G(x)$  is highly model-dependent.

### 3.6 The gluon helicity distribution from direct photon production in p-p collisions

$\Delta G(x)$  can be measured through direct (prompt) photon production in proton-proton or proton-antiproton scattering [124]. At tree level, the direct photon can be produced through two underlying subprocesses: the QCD Compton process  $qg \rightarrow q\gamma$  and the quark-antiquark annihilation  $q\bar{q} \rightarrow \gamma g$  as shown in Fig.(3.4). In proton-proton scattering the direct photon production is dominated by the QCD Compton process and hence can be used to extract the gluon distribution directly.

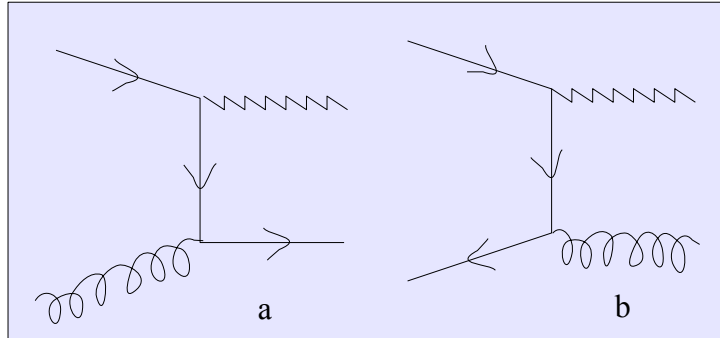


Figure (3.4): Feynman diagrams for direct photon production.

Consider the collision of hadron  $A$  and  $B$  with momenta  $P_A$  and  $P_B$ . The invariant mass of the initial state is  $s=(P_A+P_B)^2$ . We assume that the parton  $a(b)$  from the hadron  $A(B)$  carries the longitudinal momentum  $x_a P_A(x_b P_B)$ . The Mandelstam variables for the parton subprocess

$a+b \rightarrow \gamma+c$  are

$$\hat{s}=x_a x_b s, \quad \hat{t}=x_a t, \quad \hat{u}=x_b u \quad (3.25)$$

where we have neglected the hadron mass. The parton-model cross section for inclusive direct-photon production is then

$$E_\gamma \frac{d\sigma_{AB}}{d^3 p_\gamma} = \sum_{ab} dx_a dx_b f_A^a(x_a, \mu^2) f_B^b(x_b, \mu^2) E_\gamma \frac{d\hat{\sigma}_{ab}}{d^3 p_\gamma} \quad (3.26)$$

For the polarized cross section  $\Delta\sigma_{AB}$ , the parton distributions  $f_{A,B}$  are replaced by polarized distributions  $\Delta f_{A,B}$ . The parton cross sections  $\hat{\sigma}_{ab}$  are replaced by the spin-dependent cross section  $\Delta\hat{\sigma}_{ab}$ . The tree-level parton scattering cross section is

$$E_\gamma \frac{d\hat{\sigma}}{d^3 p_\gamma} = \alpha_{em} \alpha_s \frac{1}{\hat{s}} |M|^2 \delta(\hat{s} + \hat{t} + \hat{u}) \quad (3.27)$$

where the  $\delta$ -function reduces the parton momentum integration into one integration over  $x_a$  with range  $[-u/(s+t), 1]$  and

$$|M|_{qg \rightarrow \gamma q}^2 = -\frac{1}{2} \frac{\hat{s}^2 + \hat{t}^2}{\hat{s} \hat{t}}, \quad (3.28)$$

$$|M|_{q\bar{q} \rightarrow \gamma g}^2 = \frac{8}{9} \frac{\hat{u}^2 + \hat{t}^2}{\hat{u} \hat{t}},$$

For the polarized case we have the same expression as in Eq. (3.27), but with

$$|\Delta M|_{qg \rightarrow \gamma q}^2 = -\frac{1}{2} \frac{\hat{s}^2 - \hat{t}^2}{\hat{s} \hat{t}}, \quad (3.29)$$

$$|\Delta M|_{q\bar{q} \rightarrow \gamma g}^2 = -\frac{8}{9} \frac{\hat{u}^2 + \hat{t}^2}{\hat{u} \hat{t}},$$

In the energy region, where the Compton subprocess is dominant, we can write the proton-proton cross section in terms of the deep-inelastic

structure functions  $F_2$  and  $g_1$  and the gluon distributions  $G$  and  $\Delta G(x)$  [124]:

$$\begin{aligned}
E_y \frac{d\sigma_{AB}}{d^3 p_y} &= \int dx_a dx_b \left[ \frac{F_2(x_a, \mu^2)}{x_a} G(x_b, \mu^2) E_y \frac{d\hat{\sigma}_{gg}}{d^3 p_y} + (x_a \rightarrow x_b) \right] \\
E_y \frac{d\Delta\sigma_{AB}}{d^3 p_y} &= \int dx_a dx_b \left[ \frac{2g_1(x_a, \mu^2)}{x_a} \Delta G(x_b, \mu^2) E_y \frac{d\hat{\sigma}_{gg}}{d^3 p_y} + (x_a \rightarrow x_b) \right]
\end{aligned} \tag{3.30}$$

Here the factorization scale  $\mu$  is usually taken as the photon transverse momentum  $p_T$ .

The simple picture of direct photon production, described above, is more complicated due to high-order QCD corrections. Starting at next-to-leading order, the inclusive direct-photon production cross section is no longer well defined, due to the infrared divergence arising, when the photon momentum is collinear with one of the final state partons. To absorb this divergence, an additional term must be added to Eq.(3.26), which represents the production of jets and their subsequent fragmentation into photons. The total photon production cross section depends also on these unknown parton-to-photon fragmentation functions. Moreover, the separation into direct photon and jet-fragmented photon is scheme-dependent, since the parton cross section  $E_y d\hat{\sigma}_{ab}/d^3 p_y$  depends on the methods of infrared subtraction [125].

To minimize the influence of the fragmentation contribution, one can impose a cut on the experimental data [65]. The parton cross section entering Eq. (3.26) must be calculated in accordance with the cut criteria. An isolation cut has the additional benefit of excluding photons from  $\pi^0$  or  $\eta$  decay. When a high-energy  $\pi^0$  decays, occasionally the two photons cannot be resolved in a detector, or one of the photons may escape

detection. These backgrounds usually reside in the cone of a jet and are largely excluded, when an isolation cut is imposed.

The NLO parton cross sections in direct photon production have been calculated for both polarized and unpolarized scattering [125]. The comparison between the experimental data and the theory for the latter case is still controversial. While the collider data at large  $p_T$  are described very well by the NLO QCD calculation [68], the fixed-target data and collider data at low  $p_T$  are not well described by the theory. This problem can be solved by introducing a broadening of the parton transverse momentum in the initial state [69]. Theoretical ideas attempting to resolve the discrepancy include a resummation of threshold corrections [70] as well as a resummation of double logarithms, involving the parton transverse momentum [71,72]. Recently it has been shown that a combination of both effects can reduce the discrepancy considerably [73].

### 3.7 Gluon helicity distribution from jet and hadron production in p-p collisions

Jets are produced copiously in high-energy hadron colliders. The comparison between experimental data from the Tevatron and other facilities and the NLO QCD calculations are in excellent agreement. Therefore, single and/or di-jet production in polarized colliders can be an excellent tool to measure the polarized parton distributions, particularly the gluon helicity distribution [74].

There are many underlying subprocesses contributing to the leading-order jet production:

$$qq' \rightarrow qq' , \quad q\bar{q}' \rightarrow q\bar{q}' , \quad qq \rightarrow qq , \quad q\bar{q} \rightarrow q'\bar{q}' , \quad q\bar{q} \rightarrow q\bar{q} , \quad q\bar{q} \rightarrow gg , \\ gg \rightarrow q\bar{q} , \quad qq \rightarrow qq , \quad gg \rightarrow gg .$$

Summing over all pairs of initial

partons  $ab$  and subprocess channels  $ab \rightarrow cd$ , and folding in the parton distributions  $f_{a/A}(x_a)$ , etc., in the initial hadrons  $A$  and  $B$ , the net two-jet cross section is

$$\frac{d\sigma}{d^3p_c} = \sum_{abcd} \int dx_a dx_b f_{a/A}(x_a) f_{b/B}(x_b) \frac{d\hat{\sigma}}{d^3p_c}(ab \rightarrow cd) \quad (3.31)$$

For jets with large transverse momentum it is clear, that the valence quarks dominate the production. However for intermediate and small transverse momentum the jet production is overwhelmed by gluon-initiated subprocesses.

Studies of the NLO corrections are important in jet production due to the QCD structure of the jets starts at this order. For polarized scattering, this has been investigated in a Monte Carlo simulation recently [76]. The main result of the study shows that the scale dependence is greatly reduced. Even though the jet asymmetry is small, because of the large abundance of jets, the statistical error is actually very small.

Besides jets one can also look for leading hadron production, just as in electroproduction, considered previously. This is useful in particular when the jet construction is difficult, due to the limited geometrical coverage of the detectors. One generally expects, that the hadron-production asymmetry has the same level of sensitivity to the gluon density as the jet asymmetry.

## CHAPTER 4

### The Spin of the Proton

The proton contains not only three valence quarks, but also an indefinite number of gluons and quark-antiquark pairs. The sea of  $\bar{q}q$ -pairs is generated by the valence quarks emitting gluons, which then produce pairs. (fig.(4.1)). A constituent quark can be visualized as a “Quasi-particle”, which is a valence quark surrounded by a sea of gluons and  $\bar{q}q$ -pairs (fig.(4.2)). The absence of a constituent strange quark in the proton does not imply a vanishing of the matrix element  $\langle p|\bar{s}s|p\rangle$ . However the matrix element  $\langle p|s^+s|p\rangle$  must be zero, since the strangeness of proton is zero.

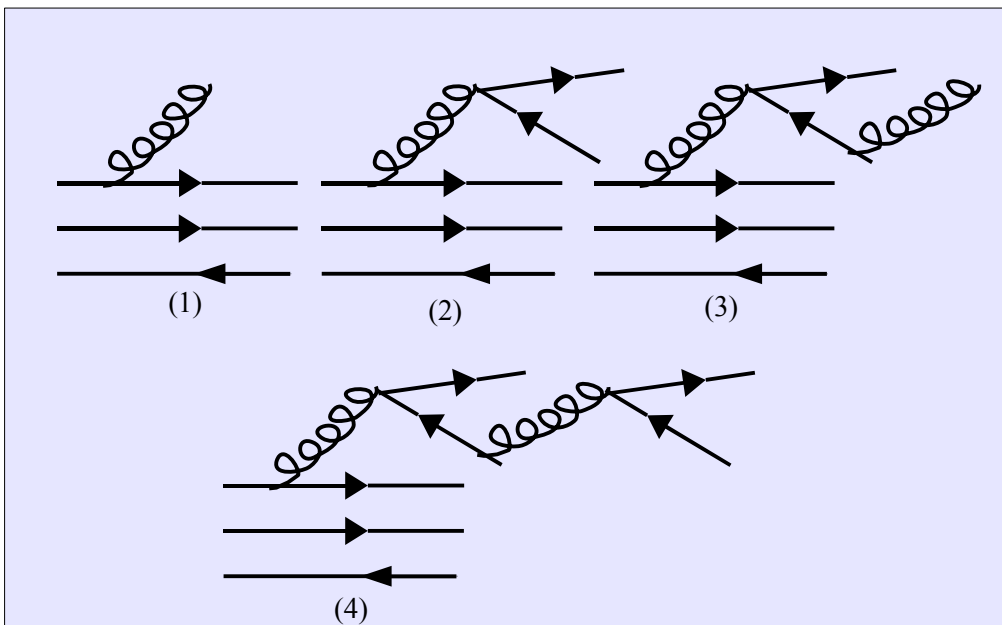


Fig.(4.1). The sea can be generated by the valence quarks emitting gluons which then produce pairs.

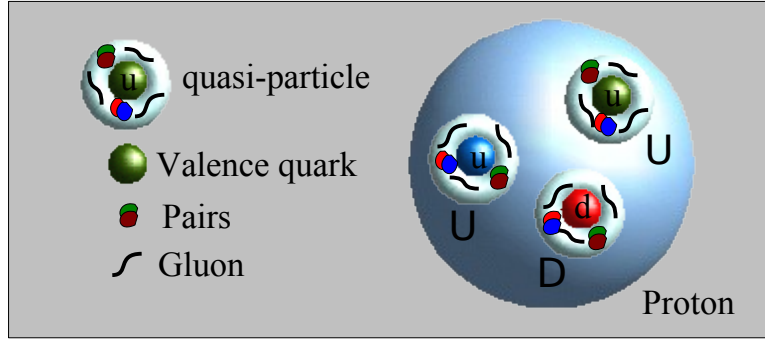


Fig.(4.2) The proton consists of two up (UU) and one down (D) constituent quark.

In order to study the spin effects of the gluons and the sea, we shall construct a phenomenological model of the spin shared by the constituents of a proton, based on the SMC[131] data of the spin dependent structure function and the knowledge of the unpolarized quark distribution functions.

Before we discuss the constituent quarks, let us summarize the results about the spin structure of the proton. We define the distribution functions of the quarks of flavor  $q$  and helicity  $+\frac{1}{2}(-\frac{1}{2})$  by  $q_+(q_-)$ . The first moment of the structure function  $g_1$ , measured in the deep inelastic scattering of polarized leptons off hadronic targets, is given by the moments of the quark densities  $\Delta q$ :

$$\int_0^1 dx g_1^p = \frac{1}{2} \left( \frac{4}{9} \Delta u + \frac{1}{9} \Delta d + \frac{1}{9} \Delta s \right) \quad (4.1)$$

where

$$\Delta u = \int_0^1 dx (u_+ - u_- + \bar{u}_+ - \bar{u}_-), \text{ etc.} \quad (4.2)$$

The spin density moments  $\Delta q$  are determined by the nucleon matrix elements of the associated axial-vector currents ( $s_\mu$ : spin vector):

$$\Delta q \cdot s_\mu = \langle p, s | \bar{q} \gamma_\mu \gamma_5 q | p, s \rangle . \quad (4.3)$$

The SMC collaboration at CERN has measured the proton structure function at  $Q^2=10 \text{ GeV}^2$  , improving the earlier SLAC-EMC measurements[131]:

$$\int_0^1 dx g_1^p = 0.142 \pm 0.008 \pm 0.011 . \quad (4.4)$$

The Bjorken sum rule[33] relates the ratio  $g_A/g_V$  of the coupling constants in the beta decay to the structure functions  $g_1^p$  and  $g_1^n$  :

$$(g_A/g_V)_{n \rightarrow p} = 6 \int_0^1 dx (g_1^p - g_1^n) = \int_0^1 dx (\Delta u - \Delta d) \quad (4.5)$$

A relation analogous to eq.(4.5) can also be written for the coupling-constant ratio  $g_A/g_V$  in the decay  $\Xi^- \rightarrow \Xi^0 e^- \bar{\nu}$  using  $SU(3)$  symmetry.

$$(g_A/g_V)_{\Xi^- \rightarrow \Xi^0} = 6 \int_0^1 dx (g_1^{\Xi^0} - g_1^{\Xi^-}) = \int_0^1 dx (\Delta d - \Delta s) \quad (4.6)$$

One finds in terms of the parameters  $F$  and  $D$ :

$$(g_A/g_V)_{n \rightarrow p} = F + D \quad , \quad (g_A/g_V)_{\Xi^- \rightarrow \Xi^0} = F - D$$

$$F + D = \int_0^1 dx (\Delta u - \Delta d) \quad (4.7)$$

$$F - D = \int_0^1 dx (\Delta d - \Delta s) \quad (4.8)$$

By summing eqs.(4.7) and (4.8) we obtain:

$$2F = \int_0^1 dx (\Delta u - \Delta s) \quad (4.9)$$

$$\Delta u = 2F + \Delta s \quad (4.10)$$

By substituting this in eq.(4.7) we obtain:

$$\Delta d=(F-D)+\Delta s \quad (4.11)$$

$$\Delta u+\Delta d-2\Delta s=3F-D \quad (4.12)$$

The parameters  $F$  and  $D$  are defined by the axial-vector matrix elements of the members of the baryon octet. From an analysis of the hyperon decays one can deduce [126]:

$$F=0.461\pm 0.014 \quad \text{and} \quad D=0.798\pm 0.013$$

Inserting these values in (4.10) and (4.11), we obtain:

$$\begin{aligned} \Delta u &= (0.922\pm 0.028) + \Delta s \quad , \\ \Delta d &= (-0.337\pm 0.019) + \Delta s \end{aligned} \quad (4.13)$$

This implies for the valence quarks:

$$\begin{aligned} \Delta u_v &= 0.922\pm 0.028 \quad , \\ \Delta d_v &= -0.337\pm 0.019 \end{aligned} \quad (4.14)$$

Inserting (4.13) in (4.1) we find:

$$\Delta s = -0.132\pm 0.046 \quad (4.15)$$

$$\begin{aligned} \Delta u &= 0.79\pm 0.054 \quad , \\ \Delta d &= -0.469\pm 0.05 \end{aligned} \quad (4.16)$$

$$\Delta \Sigma = \Delta u + \Delta d + \Delta s = 0.189\pm 0.087 \quad (4.17)$$

The analyses of Hermes [145] and COMPASS [146] give:

$$\Delta \Sigma = 0.33\pm 0.011(\text{theo.})\pm 0.025(\text{exp.})\pm 0.028(\text{evol.}) \quad (\text{HERMES})$$

$$\Delta \Sigma = 0.35\pm 0.03(\text{stat.})\pm 0.05(\text{syst.}) \quad (\text{COMPASS}) \quad (4.18)$$

It was shown[132,134] that there is an anomalous contribution to the matrix element  $\Delta \Sigma$ . In the interpretation of the EMC[1] experiment  $\Delta u$ ,  $\Delta d$  and  $\Delta s$  should be replaced by

$$\Delta \tilde{q} = \Delta q - \frac{\alpha_s}{2\pi} \Delta g , \quad (4.19)$$

where  $\Delta g$  is the gluonic helicity contribution to the proton spin. Combining this information, we obtain using  $\alpha_s(10 \text{ GeV}^2) = 0.253$  the revised estimates,

$$\begin{aligned} 0.79 \pm 0.054 &= \Delta u - \frac{\alpha_s}{2\pi} \Delta g , \\ -0.469 \pm 0.05 &= \Delta d - \frac{\alpha_s}{2\pi} \Delta g , \\ -0.132 \pm 0.046 &= \Delta s - \frac{\alpha_s}{2\pi} \Delta g \end{aligned} \quad (4.20)$$

which is still consistent with eq.(4.16), if  $\Delta g = 0$  .

The experimental determination[131] of  $\Delta s$  may be compared with two other independent determinations. One comes from an analysis[139,140] of  $\nu p$  elastic scattering[141], which leads to the value  $\Delta s = -0.15 \pm 0.08$  . This would lead to  $\Delta g = -0.45 \pm 2.3$  . However the authors of ref.[139] recommend a reanalysis of the data, as some of the assumptions made are questionable. Indeed, as shown in ref.[142], the data is equally consistent with  $\Delta s = 0$  , when the uncertainty for the proton form factor is taken into account. The other determination of  $\Delta s$  comes from a reanalysis[129] of incoherent single-pion production by neutral currents, leading to the value  $\Delta s = -0.01 \pm 0.13$  . This gives  $\Delta g = 3.0 \pm 3.4$  . For the purpose of illustration, four different characteristic values of  $\Delta g$  and hence  $\Delta s$  are chosen:

$$(i) \quad \Delta g = 3.28 \pm 1.14 , \quad \Delta s = 0.00 ,$$

- (ii)  $\Delta g=0.00$  ,  $\Delta s=-0.13\pm 0.05$  ,
- (iii)  $\Delta g=-0.45\pm 2.3$  ,  $\Delta s=-0.15\pm 0.08$  ,
- (iv)  $\Delta g=-1.19\pm 1.88$  ,  $\Delta s=-0.18\pm 0.06$  .

Case (i) with large and positive  $\Delta g$  is motivated by adapting the EMC result to the constituent quark model, whereas case (ii) with  $\Delta g=0$  is favored in some specific version of the Skyrme model[143]. The cases (iii) and (iv) with the gluon polarization opposite to the proton spin is obtained if the gluon spin component is defined via the forward matrix element of  $G\tilde{G}$  [144]. The large amount of spin carried by the gluons implies a large orbital angular momentum to compensate for it according to

$$S_z = \frac{1}{2} \Delta \Sigma + \Delta g + L_q + L_g \quad (4.21)$$

The orbital angular momenta were derived by Tang, Hoodbhoy and Xiangdong Ji using the following equation [2],

$$\frac{d}{dt} \begin{pmatrix} L_q \\ L_g \end{pmatrix} = \frac{\alpha_s(t)}{2\pi} \begin{pmatrix} -\frac{4}{3} C_F & \frac{n_f}{3} \\ \frac{4}{3} C_F & -\frac{n_f}{3} \end{pmatrix} \begin{pmatrix} L_q \\ L_g \end{pmatrix} + \frac{\alpha_s(t)}{2\pi} \begin{pmatrix} -\frac{2}{3} C_F & \frac{n_f}{3} \\ -\frac{5}{6} C_F & -\frac{11}{2} \end{pmatrix} \begin{pmatrix} \Delta \Sigma \\ \Delta g \end{pmatrix} \quad (4.22)$$

If one knows the nucleon spin composition at a perturbative scale  $Q_0^2$  , one can get the spin composition at any other perturbative scale by solving these equations. As  $Q^2 \rightarrow \infty$ , the solution becomes especially simple,

$$\frac{1}{2} \Delta \Sigma + L_q = \frac{1}{2} \frac{3n_f}{3n_f + 16} \quad ; \quad \Delta g + L_g = \frac{1}{2} \frac{16}{3n_f + 16} \quad (4.23)$$

By substituting for  $\Delta g$  and  $\frac{1}{2} \Delta \Sigma$  in this equation case (i), we get the orbital angular momenta carried by the quarks and gluons:

$$L_q=0.02\pm 0.04 \quad , \quad L_g=-2.96\pm 1.14 \quad (4.24)$$

The large orbital angular momentum is required to nearly compensate  $\Delta g$  . In order to investigate the spin sharing among the quarks and gluons in detail, one needs a parametrization of the spin densities which takes into account all the present knowledge on the structure functions. Here we present such a phenomenological model. The construction depends in particular on the unpolarized parton densities.

#### 4.1 Model of the proton spin structure

This model assumes for the unpolarized parton densities the parametrization proposed by Hwa, Zahir and X. Que-bing [127,128]. These distributions are evaluated for  $Q^2=10.7 GeV^2$  .

##### The valence quarks

The valence quark densities are given by

$$\begin{aligned} x u_v(x) &= 5.302(1-x)^{3.244} x^{0.806} \quad , \\ x d_v(x) &= 1.91(1-x)^{3.574} x^{0.636} \end{aligned} \quad (4.25)$$

Experimentally the knowledge of the nucleon spin-dependent structure functions at high momentum transfer comes from the measurement of the asymmetry “ $A$ ”, which is given by

$$A = \frac{2x g_1(x)}{F_2(x)} \quad (4.26)$$

For the proton we find:

$$2 g_1^p(x) = \frac{4}{9} \Delta u(x) + \frac{1}{9} \Delta d(x) + \frac{1}{9} \Delta s(x) \quad , \quad (4.27)$$

$$\frac{F_2^p(x)}{x} = \frac{4}{9}u(x) + \frac{1}{9}d(x) + \frac{1}{9}s(x) \quad (4.28)$$

Asymmetries for the individual quarks may also be defined:

$$A_u(x) \equiv \frac{\Delta u_v(x)}{u_v(x)} \quad , \quad A_d(x) \equiv \frac{\Delta d_v(x)}{d_v(x)} \quad (4.29)$$

The region near  $x=1$  reflects the argument[31] that the valence quark at  $x=1$  remembers the spin of the parent proton[15]. This can be achieved by choosing  $A_u(x)$  in such a way that

$$A_u(x) \rightarrow 1 \quad \text{as } x \rightarrow 1$$

$A_d(x)$  near  $x=1$  is determined by the valence quark structure of the proton, given by the naive quark model, which leads to

$$A_d(x) \rightarrow -\frac{1}{3} \quad \text{as } x \rightarrow 1 \quad .$$

The region near  $x=0$  is expected to be dominated by the sea quarks. The spin of the parent proton would no longer be related to the valence quarks. This suggests that  $A_u(x), A_d(x) \rightarrow 0$  as  $x \rightarrow 0$ . We find that the simple parametrization

$$x^{0.342} = \frac{\Delta u_v(x)}{u_v(x)} \quad , \quad -\frac{1}{3}x^{0.013} = \frac{\Delta d_v(x)}{d_v(x)} \quad (4.30)$$

satisfies all constraints mentioned above.

### The strange-sea quarks

The unpolarized strange-sea densities[127,128] are given by:

$$x s(x) = 0.168 e^{-5.6x} (1-x)^{2.59} \quad (4.31)$$

Since the large  $x$ -behavior of the spin densities of the sea quarks should be the same[138], we parametrize the spin-dependent strange-sea densities

as

$$x \Delta s(x) = 1.88 N_s x^\beta (1-x)^{8.54} \quad (4.32)$$

At small  $x$  Regge behavior suggests, that  $\beta$  is close to 0.5. The sharing of the spin between the nonstrange and strange sea quarks is assumed to be proportional to the sea production, i.e., to the unpolarized densities. This implies a common mechanism for the polarization of all flavours at some initial  $Q^2$ . Deviations from the equality would probably cause the spin dependent strange quark density to be larger in comparison to the spin averaged one, since helicity conservation is broken in the strange quark sector.

### The gluons

The unpolarized gluon densities are again taken as given in [127,128]

$$x g(x) = 0.622(1-x)^{4.83} + 1.741(1-x)^{11.82} + 13.32(1-x)^{59.69} \quad (4.33)$$

The spin densities of the gluons are parametrized in the form

$$x \Delta g(x) = N_g x^\alpha (1+ax)(1-x)^{5.9} \quad (4.34)$$

with two free parameters,  $a$  and  $\alpha$ . The first is expected to be larger than 1, and Regge arguments suggest that the second is again close to 0.5.

## 4.2 Phenomenology of the model

It is interesting that the spin sharing among the valence quarks, sea quarks and gluons is fixed for arbitrary values of the parameters  $a$ ,  $\alpha$  and  $\beta$ .

The positivity of the quark and gluon densities of given helicity  $q_+$ ,  $q_-$ ,  $g_+$  and  $g_-$  implies constraints on the parameters  $a$ ,  $\alpha$  and

$\beta$  . They can be written as  $|\Delta q_s(x, Q^2)| \leq q_s(x, Q^2)$  for the sea quarks. This implies:  $N_s \leq 0.364$  . One obtains an upper limit for  $\beta$  :  $\beta \leq 0.80$  .

Analogously for gluons the constraints imply  $|\Delta g(x, Q^2)| \leq g(x, Q^2)$  , i.e.  $\alpha \leq 0.35$  .

The parameter values, that give the best description of the data at  $Q^2=10 \text{ GeV}^2$  and the QCD parameter  $\Lambda_{QCD}=200 \text{ MeV}$  , are given as follows:

$$\beta=0.8 \quad , \quad N_s=-0.36 \quad , \quad \alpha=0.35 \quad , \quad a=3.78 \quad , \quad N_g=2.11$$

The curves representing the unpolarized and polarized valence quarks, sea quarks and gluon are plotted as a function of  $x$  shown in figures (4.3-4.6). Below I will discuss the measurements of the gluon distribution.

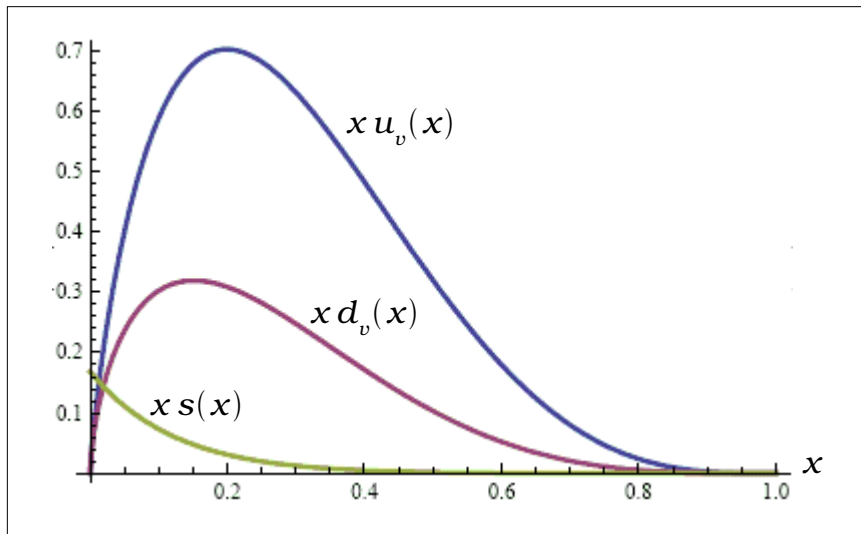


Fig.(4.3) Unpolarized functions of the valence, sea quarks and gluon plotted as function of  $x$ .

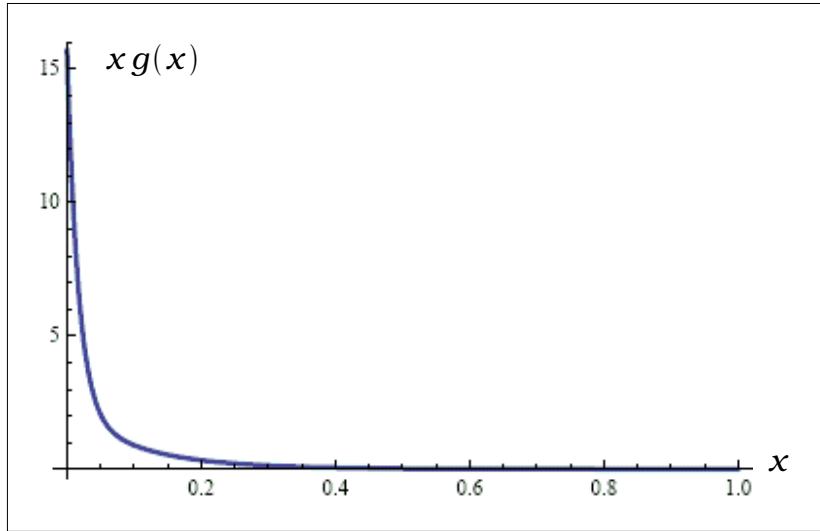


Fig.(4.4) Unpolarized functions of the gluon plotted as function of x.

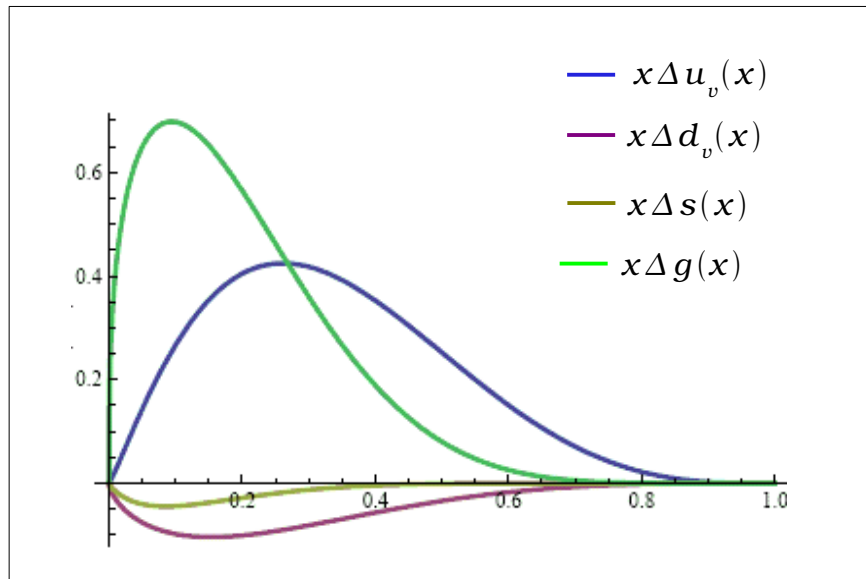


Fig.(4.5) spin densities of the valence, sea quarks and gluon plotted as function of x.

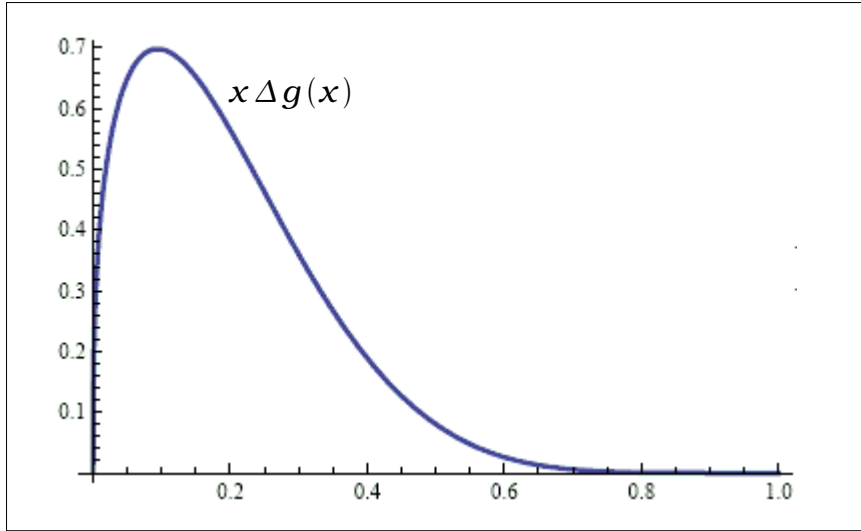


Fig.(4.6) Spin density of the gluon plotted as function of x.

### 4.3 Experimental Measurements of the gluon distribution

The first information on the gluon helicity distribution  $\Delta g$  has come from NLO fits to inclusive deep-inelastic scattering data. The semi-inclusive data from the HERMES experiment indicates a positive gluon polarization, also other measurements from COMPASS at CERN, polarized RHIC, and polarized HERA. All data indicate, that the gluon polarisation is small, compared to earlier expectations, but it still can give a large contribution to the nucleon spin.

In Ref.[30] the HERMES collaboration reported a first measurement of the longitudinal spin asymmetry  $A_{ll} = -0.28 \pm 0.12 \pm 0.02$  in the photoproduction of pairs of hadrons with high transverse momentum  $P_T$ , which translate into a  $\langle \Delta g/g \rangle = 0.4 \pm 0.18 \pm 0.03$  at an average  $\langle x \rangle = 0.17$ . HERMES presented a new analysis of  $\Delta g/g$ , [34] including the deuteron data. Their most precise result comes from the

inclusive hadron asymmetries. A polarised gluon distribution function is fitted to  $\Delta g/g$  in four  $p_T$  bins in the range  $1.05 GeV < p_T < 2.5 GeV$  (fig.(4.7)). The larger 1999 HERMES result [30] had been obtained from hadron pairs. The data are included in the new analysis.

COMPASS performed a separate analysis for hadron pairs produced at  $Q^2 \geq 1 GeV^2$  and  $Q^2 < 1 GeV^2$ . The inclusion of the 2004 deuteron data in the low  $Q^2$  analysis[23] yielded an about 1.5 times more precise preliminary result. The gluon polarisation from the high and low  $Q^2$  analyses is compatible with zero and probes the region around  $x_g \approx 0.1$ . Open charm production is considered to be the most model-independent tool to study the gluon polarisation. Due to the small initial cross-sections and the small branching ratio in the decay  $D^0 \rightarrow K \pi$  the measurement of an asymmetry in  $D$  meson production is a real challenge. COMPASS has determined  $\Delta g/g$  from this asymmetry.

One of the primary goals of the RHIC spin experiments was to determine the polarized gluon distribution, using the direct photon, jet, and heavy quark production. This was done on the inclusive direct photon events (PHENIX) and photon-plus-jet events (STAR). At the present luminosities and a *c.m.* energy of  $\sqrt{s} = 200 GeV$  the most promising channels are the inclusive  $\pi^0$  and jet [133] longitudinal double-spin asymmetries  $A_{ll}$  measured by PHENIX and STAR. The present status of these measurements is shown in Fig.(4.8). Also shown are the NLO calculations [135,136] using the GRSV set of PDFs [137] for four different assumptions for the gluon polarisation: the best fit to the world data (GRSV-std), and  $\Delta g = -g, 0, g$  at  $Q_0^2 = 0.3 GeV^2$ . As first observed by COMPASS [23], the data rule out the  $\Delta g = g$  scenario, while the other scenarios are still possible. The dependence of the asymmetry

$A_{ll}$  on  $\Delta g/g$  contains a quadratic term, which makes it at present impossible to determine the sign of  $\Delta g/g$  from the RHIC data. Very encouraging are the prospects for the data taken in 2006. The average beam polarisation  $P_B$  improved from 46% in 2005 to 62%. Also the luminosity increased. The table(4.2) shows the leading order measurements of  $\Delta g/g$ .

TABLE (4.1). Leading order measurements of  $\Delta g/g$  :

Experiment	Method	$\langle x \rangle$	$\Delta g/g$
COMPASS [23]	hadron pairs ( $Q^2 < 1$ )	0.085	$0.016 \pm 0.058 \pm 0.055$
COMPASS[23]	hadron pairs ( $Q^2 > 1$ )	0.13	$0.06 \pm 0.131 \pm 0.06$
COMPASS[23]	open charm	0.15	$-0.57 \pm 0.41$
HERMES[30]	hadron pairs	0.17	$0.41 \pm 0.18 \pm 0.03$
HERMES[34]	incl. hadrons	0.22	$0.071 \pm 0.034^{+0.0105}_{-0.1270}$
SMC[130]	hadron pairs ( $Q^2 > 1$ )	0.07	$-0.20 \pm 0.28 \pm 0.10$

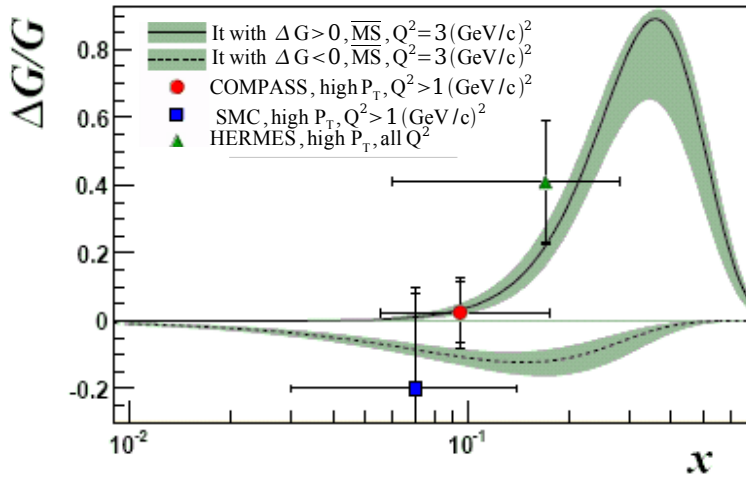


Fig.(4.7). Gluon polarisation  $\Delta g/g$  as function of  $x$  at  $Q^2=Q_o^2$  obtained by NLO QCD fits (bands) and from LO analysis of hadron helicity asymmetries (symbols). It is from COMPASS QCD fits [21] including the new COMPASS deuteron data. ( $Q^2=3 GeV^2$ ).

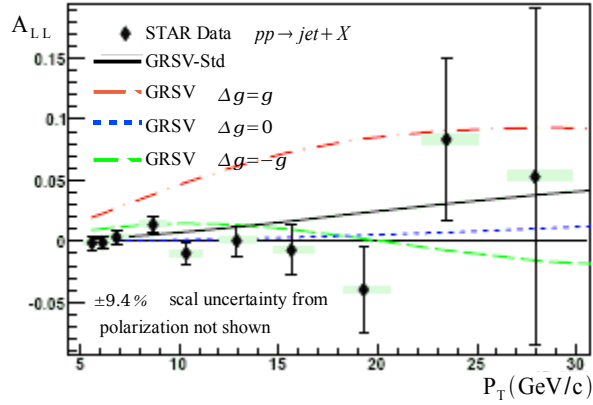


Fig.(4.8).  $A_{ll}$  for inclusive jet production at STAR as function of  $p_T$ [14].

#### 4.4 Constituent Quarks in QCD

The magnetic moment of a spin 1/2 pointlike particle in the Dirac theory is given by:

$$\mu = \left(\frac{e\hbar}{mc}\right) s = \left(\frac{e\hbar}{mc}\right) \frac{1}{2} \sigma \quad (4.35)$$

where  $\sigma$  is the Pauli matrix. The magnetic moment depends on the mass, the spin, and the electric charge of the particle. If baryons ( $s=1/2, 3/2, \dots$ ) are made up of quarks (spin 1/2 fermions), then we should be able to calculate the magnetic moments in terms of the magnetic moments of the quarks.

In the quark model the space, spin, and flavor (isotopic spin) parts of the wave function are symmetric under the exchange of two quarks. The color part of the wave function must then be antisymmetric to satisfy the Pauli Principle. Since we are dealing with ground states ( $L=0$ ), the space part of the wave function should be symmetric.

The spin of the proton (spin 1/2) is a function of the spins of the three quarks. From the table of Clebsch-Gordan coefficients we find:

$$|1/2 \ 1/2\rangle = \sqrt{\frac{2}{3}}|1 \ 1\rangle|1/2 \ -1/2\rangle - \sqrt{\frac{1}{3}}|1 \ 0\rangle|1/2 \ 1/2\rangle$$

Also we have:

$$\begin{aligned} |1 \ 1\rangle &= |1/2 \ 1/2\rangle|1/2 \ 1/2\rangle \\ |1 \ 0\rangle &= \sqrt{\frac{1}{2}}|1/2 \ 1/2\rangle|1/2 \ -1/2\rangle + \sqrt{\frac{1}{2}}|1/2 \ -1/2\rangle|1/2 \ 1/2\rangle \end{aligned}$$

Using the notation:

$$|1/2 \ 1/2\rangle = \uparrow \quad \text{and} \quad |1/2 \ -1/2\rangle = \downarrow$$

the spin part of the wave function can be written as:

$$|1/2 \ 1/2\rangle = -\sqrt{\frac{2}{3}}[\uparrow\uparrow\downarrow] - \sqrt{\frac{1}{3}} \cdot \sqrt{\frac{1}{2}}[\uparrow\downarrow\uparrow + \downarrow\uparrow\uparrow] = \sqrt{\frac{1}{6}}[2\uparrow\uparrow\downarrow - \uparrow\downarrow\uparrow - \downarrow\uparrow\uparrow] \quad (4.36)$$

This wave function is symmetric under the interchange of the first two spins. Due to isospin the two  $u$  quarks are in a symmetric  $I=1$  state. With respect to the spin the  $u$  quarks must be in a symmetric state. This implies that in the  $2\uparrow\uparrow\downarrow$  term in the spin function the two  $\uparrow\uparrow$  are the  $u$  quarks. In the other terms the  $u$ 's have opposite  $s_z$ 's.

We need to construct a symmetric spin and flavor (isospin) proton wave function. We can write the symmetric spin and flavor (isospin) proton wave function as:

$$\psi = \sqrt{\frac{1}{18}} \begin{pmatrix} 2u\uparrow u\uparrow d\downarrow + 2d\downarrow u\uparrow u\uparrow + 2u\uparrow d\downarrow u\uparrow - u\downarrow d\uparrow u\uparrow - u\uparrow u\downarrow d\uparrow \\ -u\downarrow u\uparrow d\uparrow - d\uparrow u\downarrow u\uparrow - u\uparrow d\uparrow u\downarrow - d\uparrow u\uparrow u\downarrow \end{pmatrix} \quad (4.37)$$

This wave function is symmetric under the interchange of *any* two quarks. It is also obtained in the SU(6)-model of the baryons.

The theoretical assumption, which allow to derive the ratio of the magnetic moments of the neutron and proton, is[147]:

- (i) The magnetic moment of a baryon is the sum of the magnetic

moments of the quarks.

- (ii) The quark spins, which determine the directions of the quark magnetic moments, are given by the nonrelativistic SU(6) wave function, given above.

The magnetic moment of the proton is

$$\vec{\mu} = \vec{\mu}_1 + \vec{\mu}_2 + \vec{\mu}_3$$

where  $\vec{\mu}$  is the magnetic moment operator for the quarks.

$$\langle u | \vec{\mu} | u \rangle = \vec{\mu}_u = \text{magnet moment of u quark}$$

$$\langle d | \vec{\mu} | d \rangle = \vec{\mu}_d = \text{magnet moment of d quark}$$

$$\langle u s_z | \vec{\mu} | u s_z \rangle = \mu_{u s_z} = \frac{2}{3} \cdot \frac{e \hbar}{m_u c} \cdot s_z, \text{ with } s_z = \pm 1/2$$

$$\langle d s_z | \vec{\mu} | d s_z \rangle = \mu_{d s_z} = -\frac{1}{3} \cdot \frac{e \hbar}{m_d c} \cdot s_z, \text{ with } s_z = \pm 1/2,$$

$$\langle u s_{z=1/2} | \vec{\mu} | u s_{z=-1/2} \rangle = 0, \text{ etc...}$$

For the proton ( $uud$ ) we find:

$$\begin{aligned} \langle \psi_p | \vec{\mu} | \psi_p \rangle &= \frac{1}{18} (24 \vec{\mu}_{u,1/2} + 12 \vec{\mu}_{d,-1/2} + 6 \vec{\mu}_{d,1/2}) \\ &= \frac{1}{18} (24 \vec{\mu}_{u,1/2} - 6 \vec{\mu}_{d,1/2}) = \frac{4}{3} \vec{\mu}_{u,1/2} - \frac{1}{3} \vec{\mu}_{d,1/2} \end{aligned} \quad (4.38)$$

(we used  $\vec{\mu}_{d,-1/2} = -\vec{\mu}_{d,1/2}$  )

For the neutron ( $udd$ ) we obtain:

$$\langle \psi_n | \vec{\mu} | \psi_n \rangle = \frac{4}{3} \vec{\mu}_{d,1/2} - \frac{1}{3} \vec{\mu}_{u,1/2} \quad (4.39)$$

In the limit  $m_u = m_d = m$  we obtain:

$$\langle \psi_p | \mu | \psi_p \rangle = \frac{4}{3} \cdot \frac{2}{3} \cdot \frac{e \hbar}{m c} \cdot \frac{1}{2} - \frac{1}{3} \cdot \left( -\frac{1}{3} \cdot \frac{e \hbar}{m c} \cdot \frac{1}{2} \right) = \frac{\hbar e}{2 m c} (1) \quad (4.40)$$

$$\langle \psi_n | \mu | \psi_n \rangle = \frac{4}{3} \cdot \left( -\frac{1}{3} \cdot \frac{e\hbar}{mc} \cdot \frac{1}{2} \right) - \frac{1}{3} \cdot \frac{2}{3} \cdot \frac{e\hbar}{mc} \cdot \frac{1}{2} = \frac{\hbar e}{2mc} \left( -\frac{2}{3} \right) \quad (4.41)$$

The ratio of the magnetic moments is:

$$\frac{\langle \psi_p | \mu | \psi_p \rangle}{\langle \psi_n | \mu | \psi_n \rangle} = \frac{\mu_p}{\mu_n} = -\frac{3}{2} \quad (4.42)$$

The magnetic moments calculated above are in good agreement with the experimental data (table (4.2)).

Table (4.2) Magnetic moments of proton and neutron [148].

Nucleon	Moment	Experiment
p	$\frac{4}{3}\mu_u - \frac{1}{3}\mu_d$	2.793
n	$\frac{4}{3}\mu_d - \frac{1}{3}\mu_u$	-1.913

In the table (4.2) the numerical values are given as multiples of the

magneton,  $\frac{e\hbar}{2m_p c} = 3.152 \times 10^{-18} \text{ Mev/gauss}$ .

Thus the constituent quark model and the SU(6) wave function for the nucleon works very well for the magnetic moments. The prediction for the ratio

$$\frac{\mu_p}{\mu_n} = -\frac{3}{2}$$

agrees with the experimental result:

$$\frac{\mu_p}{\mu_n} = -1.46$$

In addition the SU(6) proton spin wave function eq.(4.37) gives the polarization of the quarks as,

$$\Delta u = \frac{4}{3}, \quad \Delta d = -\frac{1}{3}, \quad \Delta s = 0$$

Since the magnetic moment is proportional to the spin, the proton magnetic moment is then given by,

$$\mu_p = \frac{4}{3}\mu_u - \frac{1}{3}\mu_d \quad (4.43)$$

It is easy to see that all the baryon magnetic moments can be expressed in terms of quark magnetic moments,  $\mu_u$ ,  $\mu_d$  and  $\mu_s$ . A fit to the experimental data gives [17]

$$\mu_u = 1.852\mu_N, \quad \mu_d = -0.972\mu_N, \quad \mu_s = -0.613\mu_N$$

where  $\mu_N$  is the nuclear magneton. For elementary Dirac particles we

have  $\mu_q = \frac{e_q}{2m_q}$  with  $e_q$  the charge of the quark. Thus we obtain the quark masses:

$$m_u = 338 \text{ Mev}, \quad m_d = 322 \text{ Mev}, \quad m_s = 510 \text{ Mev}$$

These are the constituent quark masses.

We mentioned that the constituent quarks have an internal structure on their own. Thus a constituent quark has a dynamical structure, and we can introduce notions like the quark or gluon distributions inside a constituent quark.

Let us consider a U constituent quark. It is described by the distribution functions

$$u_+(x), u_-(x), d_+(x), d_-(x), s_+(x) \text{ and } s_-(x).$$

The flavor conservation laws imply sum rules for the distribution functions in a U-quark:

$$\int_0^1 dx (u_+ + u_- - \bar{u}_+ - \bar{u}_-) = 1 \quad (4.44)$$

$$\int_0^1 dx (d_+ + d_- - \bar{d}_+ - \bar{d}_-) = 0 \quad (4.45)$$

These sum rules are analogous to the Adler sum rules for the nucleon. We proceed to discuss the analogue of the Bjorken sum rule:

$$\int_0^1 dx [(u_+ + \bar{u}_+) - (u_- + \bar{u}_-)] = g_a^u \quad (4.46)$$

$$\int_0^1 dx [(d_+ + \bar{d}_+) - (d_- + \bar{d}_-)] = g_a^d$$

On the right side of the integral appears the axialvector coupling constant of the constituent quark. It is defined by the matrix element of the axial vector current  $\bar{u}(x)\gamma_\mu\gamma_5 u(y)$  or  $\bar{d}(x)\gamma_\mu\gamma_5 d(y)$ . We can also consider the sum rule for the isovector operator:

$$\int_0^1 dx \{[(u_+ + \bar{u}_+) - (u_- + \bar{u}_-)] - [(d_+ + \bar{d}_+) - (d_- + \bar{d}_-)]\} = g_a^u - g_a^d = g_a \quad (4.47)$$

and the sum rule, related to the matrix element of the isosinglet current:

$$\int_0^1 dx \{[(u_+ + \bar{u}_+) - (u_- + \bar{u}_-)] + [(d_+ + \bar{d}_+) - (d_- + \bar{d}_-)]\} = g_a^u + g_a^d = \Sigma \quad (4.48)$$

The parameter  $\Sigma$  can be viewed as the contribution of the u- and d-quarks to the U-spin. If we identify the constituent quarks with the current quarks, seen in deep inelastic scattering, the sum rules are trivial. The antiquark densities vanish as well as all d-densities. Furthermore  $u_-$  is zero.

$$\int_0^1 dx u_+ = 1 \quad , \quad g_a = \Sigma = 1 \quad , \quad d_+ = d_- = \bar{d}_+ = \bar{d}_- = u_- = \bar{u}_+ = 0 \quad (4.49)$$

If we assume this approximation and apply it to the nucleon, we would obtain, using the SU(6) wave functions:

$$|g_a/g_v| = 5/3 \quad (4.50)$$

But the experiments give:

$$|g_a/g_v| \approx 1.26 \quad (4.51)$$

Thus the axial-vector charge is reduced from 5/3 by about 24 percent. In the constituent quark model this reduction would also apply to the constituent quarks. In this case we obtain for a constituent quark  $g_a^u \approx 0.76$  .

How can one understand this reduction in quantum chromodynamics? In QCD there are, besides the quarks, also gluons. Thus far they did not appear in the calculations. The gluons should also contribute to the spin. A constituent quark can appear at short distances as a quark, carrying spin 1/2, or as a quark, carrying spin -1/2, plus a gluon, carrying spin +1. This effect can be calculated in perturbation theory, but such a calculation would not be reliable, since we are investigating a bound state effect, which depends on large distances, where perturbation theory does not apply.

A constituent quark is described by the quark distribution functions  $u_+$  and  $u_-$  , if we neglect the antiquarks. The sum rule reduces to the integral:

$$\int_0^1 dx (u_+ - u_-) = g_a^u \approx 0.76 \quad (4.52)$$

and we obtain:

$$\int_0^1 dx u_+ = \frac{1}{2}(1 + g_a) \approx 0.88$$

$$\int_0^1 dx u_- = \frac{1}{2}(1 - g_a) \approx 0.12 \quad (4.53)$$

The spin of a constituent U-quark is provided by the u-quark, making up

76% of the spin, and the remaining 24% must be provided by the gluons. In this way we understand, why the axialvector charge of the proton is not 5/3, as expected in the naive quark model.

We note that this modification of the wave function of a nucleon does not affect the ratio of the magnetic moments of the nucleon. We still obtain for the ratio  $r$  of the magnetic moments of the proton and the neutron:  $r = -3/2$ .

According to the experiments the quarks contribute only about 30 % to the spin of the proton. However we obtain about 76%, and the question arises, how the reduction from 76% to 30% can arise. It should be due to the contributions of pairs of quarks and antiquarks.

The divergence of the axialvector current of a particular quark flavor  $q$  has an anomaly due to the gluons:

$$\partial^\mu (\bar{q} \gamma_\mu \gamma_5 q) = -\frac{g^2}{32 \pi^2} \varepsilon_{\alpha\beta\gamma\delta} G^{\alpha\beta} G^{\gamma\delta} \quad (4.54)$$

Thus in the limit of vanishing quark masses the isosinglet current has an anomaly. The anomaly implies that the matrix element of the isosinglet current, given by  $\Sigma$ , is not equal to the matrix element of the isotriplet current. The integral over the distribution functions of the d-quarks is given by the difference:

$$\int_0^1 dx (d_+ + \bar{d}_+ - d_- - \bar{d}_-) = \frac{1}{2} (\Sigma - g_a) \quad (4.55)$$

The difference  $\Sigma - g_a$  is given by the matrix element of the d-quark axial-vector current in the U-quark. This matrix element vanishes in the model, discussed above, and  $\Sigma$  would be equal to the axial charge  $g_a$ . In reality this is not true. The observed value of  $\Sigma$  for a constituent

quark is about 0.30 , and  $g_a$  is 0.76. Thus we obtain for the d-integral

$$\frac{1}{2}(\Sigma - g_a) = -0.23 \quad (4.56)$$

Due to the QCD-anomaly quark-antiquark-pairs are created in the U-quark. This is a nonperturbative effect. These pairs are polarized, cancelling partially the spin of the U-quark.

The sum rule for the d-distribution functions implies that the integral of the polarized  $\bar{d}d$  -pairs is nonzero, but it is not implied that the sum of the positively polarized  $\bar{d}d$  -pairs is nonzero. It is possible, that there are no positively polarized  $\bar{d}d$  -pairs.

The generation of the  $\bar{d}d$  -pairs is directly related to the gluon anomaly, i.e. to the gluons, and not to the valence u quark. Thus we expect that the negatively polarized d quarks and antiquarks have the same distribution function, since the gluon anomaly does not differentiate between quarks and antiquarks.

The pair creation through the gluon anomaly should be flavor symmetric, i.e. we expect also the creation of u-pairs. In particular the negatively polarized anti-u-quarks and the negatively polarized anti-d-quarks should have the same distribution function. The simplest way to obey the sum rules is to take:

$$\bar{u}_+ = 0 \quad , \quad d_+ = \bar{d}_+ = 0 \quad , \quad d_- = \bar{d}_- = \bar{u}_- \quad (4.57)$$

We find:

$$\int_0^1 dx (d_- + \bar{d}_-) = -\frac{1}{2}(\Sigma - g_a) \simeq 0.22 \quad (4.58)$$

$$\int_0^1 dx \bar{u}_- = -\frac{1}{4}(\Sigma - g_a) \simeq 0.11 \quad (4.59)$$

$$\int_0^1 dx (u_+ - u_- - \bar{u}_-) = \frac{1}{2}(\Sigma + g_a) \simeq 0.53 \quad (4.60)$$

Let us summarize this model for the nucleon spin. The proton is composed of three constituent quarks, which have an internal structure. The quarks contribute to the spin only about 30 percent, both for the proton as well as for the constituent quarks. We attribute the failure of the prediction of SU(6) symmetry for the axial charge to a spin flip effect expected in QCD. This effect would reduce the spin contribution of the quarks from 100 percent to 76 percent. A further reduction is provided by the quark-antiquark-pairs, which reduce the contribution of the quarks down to 30%. Thus the gluons will contribute about 70 percent to the spin of a proton.

## SUMMARY AND CONCLUSION

The goal of this thesis was study the spin structure of the proton in the theory of the QCD. We have calculated the quark helicity contribution to the nucleon spin. We have tried to understand the flavor and sea separation of the quark helicity distributions, and of the polarized gluon distribution. I have described why polarized constituent quarks should be surrounded by a cloud of polarized quark-antiquark pairs. Our reasoning was entirely based on phenomenological arguments. It would be interesting to see how these polarized pairs are generated dynamically, via the non-perturbative effects, which are responsible also for the QCD mass gap and the breaking of the chiral symmetry in the axial-singlet channel. An explicit dynamical model along these lines is not yet available. The generation of polarized  $\bar{q}q$  -pairs can be studied in the lattice approach to QCD.

## **ACKNOWLEDGMENTS**

It was a great pleasure for me to work in the High Energy Physics group of the Ludwig-Maximilians-Universität München for more than three years.

I like to present my sincere thank and deep appreciation to my supervisor Prof. Dr. Harald Fritzsch.

My thanks also extend to Prof. Dr. Gerhard Buchalla for his encouragement. Similarly my thanks are for all the staff members and colleagues of the Chair of High Energy Physics who helped from time to time, especially Dr. Michael Spannowsky for his help from the first day, when I came in München, and Abdul Aziz Bhatti.

Above all, I am highly indebted and thankful to my mother El-Hajja Hafidha, who constantly supported me by her continuous love and prayers.

## REFERENCES

---

1. European Muon Collaboration (J. Ashman et al.) Nucl. Phys. B328: 1,1989.
2. Xiangdong Ji, Jian Tang and Hoodbhoy, Phys. Rev. Lett. 76:740-743,1996.
3. Aneesh V. Manohar, Lectures given at Lake Louise Winter Inst., Lake Louise, Canada, Feb 23-29, 1992. [hep-ph /9204208].
4. FINESS Collaboration (L. Bugel et al.), Fermilab Proposal hep-ex/042007.
5. J. Koryluk for the STAR collaboration) in these proceedings. hep-ex/0512040.
6. PHENIX Collaboration (S.S. Adler et al.) Phys. Rev. Lett. 93 202002 (2004).
7. H. Fritzsch, M. Gell-Mann, H. Leutwyler, Phys. Lett. B47 (1973) 365.
8. G. Veneziano, Nucl. Phys. B159, 213 (1979).
9. J. D. Bjorken, Phys.Rev.179:1547-1553,1969.
10. E. Leader and E. Predazzi, Cambridge, Uk: Univ. Pr. (1982) 498p.
11. M. G. Doncel and E. De Rafael, Nuovo Cimento 4A (1971) 363.
12. M. Anselmino and E. Leader, Z. Phys. C 41 (1988) 239.
13. H. Cheng and E Fischbach, Phys. Rev. D19 (1979) 860.
14. D. J. E. Callaway and S. D. Ellis, Phys. Rev. D29 (1984) 567.
15. G. R. Farrar and D. R. Jackson, Phys. Rev. Lett. 35, 1416 (1975).
16. J. Ellis and R. L. Jaffe, Phys. Rev. D9 (1974) 1444 and D10 (1974) 1669.
17. Particle Data Group, Phys. Rev. D54, 1 (1996).
18. J. Kodaira et al, Phys. Rev. D20 (1979) 627.
19. M. Anselmino, A. Efremov, E. Leader, Phys. Rept. 261: 1–124, 1995.

20. B. Lampe, E. Reya, Phys. Rept. 332: 1–163, 2000.
21. K. Rith, Spin Asymmetries in Deep Inelastic Electron-Nucleon Scattering: Selected HERMES Results, Prog. Part. Nucl. Phys. 49 (2002) 245–324.
22. K. Rith, Quark-Gluon Structure of the Nucleon, in: F. Lenz et al. (Ed.), Lectures on QCD, Springer Verlag, 1997.
23. E. S. Ageev et al. [COMPASS Collaboration], Phys. Lett. B 633, 25 (2006) [arXiv:hep-ex/0511028].
24. F. Halzen, A. Martin, Quarks and Leptons, John Wiley & Sons, 1984.
25. M. Gell-Mann, Phys. Lett. 8: 214 –215, 1964.
26. G. Zweig, An SU(3) Model for Strong Interaction Symmetry and its Breaking. 2 , CERN-TH-412.
27. R. P. Feynman, Phys. Rev. Lett. 23 (1969) 1415–1417.
28. J. D. Bjorken, E. A. Paschos, Phys. Rev. 185 (1969) 1975– 1982.
29. R. Devenish, A. Cooper-Sarkar, Deep Inelastic Scattering, Oxford University Press, 2004.
30. HERMES , A. Airapetian et al., Phys. Rev. Lett. 84 , 2584 (2000) [arXiv:hep-ex/9907020].
31. R. P. Feynman, “Photon-Hadron Interactions” (Benjamin, New York, 1972).
32. S. Eidelman et al., Review of Particle Physics, Physics Letters B 592 (2004) 1. <http://pdg.lbl.gov>.
33. J. D. Bjorken, Phys. Rev. 148, 1467 (1966).
34. COMPASS Collaboration, V. Yu. Aleksakhin et al. Phys. Lett., [arXiv:hep-ex/0609038].
35. F. E. Close and D. Sivers, Phys. Rev. Lett. 39, 1116-1120, 1977.
36. J. Ellis and R.L. Jaffe, Phys. Rev. D9, 1444 (1974); 10, 1669 (E) (1974).
37. J. Kodaira, S. Matsuda, T. Muta, K. Sasaki, T. Uematsu, Phys. Rev. D20 (1979) 627.

38. J. Kodaira, Nucl. Phys. B165 (1980) 129.
39. J. Ashman et al., Phys. Lett. B206 (1988) 364.
40. J. Ashman et al., Nucl. Phys. B328 (1989) 1.
41. J. R. Ellis, R. L. Jaffe, Phys. Rev. D9 (1974) 1444.
42. B. Adeva et al., Phys. Rev. D58 (1998) 112002.
43. M. Hirai, S. Kumano, N. Saito, Phys. Rev. D69 (2004) 054021.
44. A. Airapetian et al., Phys. Rev. D71 (2005) 012003.
45. T. D. Averett, Nucleon Spin Structure Functions  $g_1$  and  $g_2$  from Polarized Inclusive Scattering, AIP Conf. Proc. 675 (2003) 88–97.
46. J. Hannappel, Measurement of the Spin Structure of the Deuteron at COMPASS, talk given at: DIS05 - 13th International Workshop on Deep Inelastic Scattering, Madison, Wisconsin USA.
47. M. Glück, E. Reya, M. Stratmann, W. Vogelsang, Phys. Rev. D63 (2001) 094005.
48. J. Blümlein, H. Böttcher, Nucl. Phys. B636 (2002) 225–263.
49. J. D. Bjorken, Phys. Rev. D1 (1970) 1376–1379.
50. Panying Chen<sup>1</sup> and Xiangdong Ji, Phys. Lett. B660:193-196, 2008.
51. D. Adams et al., Phys. Rev. D56 (1997) 5330–5358.
52. G. Altarelli, G. Parisi, Nucl. Phys. B126 (1977) 298.
53. V. N. Gribov, L. N. Lipatov, Sov. J. Nucl. Phys. 15 (1972) 438–450.
54. Y. L. Dokshitzer, Sov. Phys. JETP 46 (1977) 641–653.
55. G. Altarelli, R. D. Ball, S. Forte, G. Ridolfi, Acta Phys. Polon. B29 (1998) 1145–1173.
56. W. Vogelsang, Phys. Rev. D54 (1996) 2023–2029.
57. W. Vogelsang, Nucl. Phys. B475 (1996) 47–72.
58. R. Mertig, W. L. van Neerven, Z. Phys. C70 (1996) 637–654.
59. M. Glück, E. Reya, M. Stratmann, W. Vogelsang, Phys. Rev. D53

- (1996) 4775–4786.
60. E. Leader, A. V. Sidorov, D. B. Stamenov, *Eur. Phys. J. C* 23 (2002) 479–485.
  61. E. Leader, A. V. Sidorov, D. B. Stamenov, *Phys. Rev. D* 58 (1998) 114028.
  62. E. Leader, A. V. Sidorov, D. B. Stamenov, *Phys. Lett. B* 462 (1999) 189–194.
  63. S. L. Adler, *Phys. Rev.* 177 (1969) 2426–2438.
  64. R. D. Carlitz, J. C. Collins, A. H. Mueller, *Phys. Lett. B* 214 (1988) 229.
  65. S. D. Ellis and S. Soper, *Phys. Rev. D* 48 , 3160 (1993).
  66. S. L. Adler, W. A. Bardeen, *Phys. Rev.* 182 (1969) 1517–1536.
  67. C. S. Lam, B.-A. Li, *Phys. Rev. D* 25 (1982) 683–694.
  68. (D0) Abbott et al., *Phys. Rev. Lett.* 84, 2786 (2000).
  69. L. Apanasevich et al., *Phys. Rev. D* 59, 074007 (1999).
  70. H.-L. Lai and H.-n. Li, *Phys. Rev. D* 58, 114020 (1998).
  71. E. Laenen, G. Orderda, and G. Sterman, *Phys. Lett. B* 438, 173 (1998).
  72. S. Catani, M. L. Mangano, and P. Nason, *JHEP* 9807, 024 (1998).
  73. E. Laenen, G. Sterman, and W. Vogelsang, *Phys. Rev. Lett.* 84, 4296 (2000).
  74. C. Bourrely, J. Ph Guillet, and J. Soffer, *Nucl. Phys. B* 361 , 72 (1991); P. Chiappetta, P. Colangelo, J. Ph Guillet, and G. Nardulli, *Z. Phys. C* 59 , 629 (1993); J. Soffer and J. M. Virey, *Nucl. Phys. B* 509 , 297 (1998).
  75. (E155) P. L. Anthony et al., hep-ph/0007248.
  76. D. de Florian, S. Frixione, A. Signer, and W. Vogelsang, *Nucl. Phys. B* 539, 455 (1999).
  77. G. t. Hooft and M. Veltman, *Nucl. Phys. B* 44, 189 (1972).
  78. R. Mertig and W. L. van Neerven, *Z. Phys. C* 70 , 637 (1996).

79. W. Vogelsang, Nucl. Phys. B 475, 47 (1996).
80. R. D. Ball, S. Forte and G. Ridolfi, Phys. Lett. B 378 , 255 (1996).
81. G. Altarelli, R.D. Ball, S. Forte and G. Ridolfi, Acta Phys. Polon. B29 , 1145 (1998).
82. R. D. Carlitz, J. C. Collins and A. H. Mueller, Phys. Lett. B 214 , 229 (1988).
83. E. Leader, A. V. Sidorov and D. B. Stamenov, Phys. Lett. B 445 , 232 (1998).
84. H-Y Cheng, Phys. Lett. B 427 , 371 (1998).
85. D. Muller and O. V. Teryaev, Phys. Rev. D 56 , 2607 (1997).
86. E. Leader, A. V. Sidorov and D. B. Stamenov, Phys. Rev. D 58, 114028 (1998).
87. V. N. Gribov and L. N. Lipatov, Sov. J. Nucl. Phys. 15 , 138 (1972), Yu. L. Dokahitzer, Sov. Phys. JETP 16 , 161 (1977), G. Altarelli and G. Parisi, Nucl. Phys. B 126 , 298 (1977).
88. G. Altarelli, S. Forte and G. Ridolfi, Nucl. Phys. B 534, 277 (1998).
89. M. Gluck et al., Phys. Rev. D 53 , 4775 (1996).
90. T. Gehrmann and W. J. Stirling, Phys. Rev. D 53 , 6100 (1996).
91. (SMC) B. Adeva et al., Phys. Lett. B 58 , 112002 (1998).
92. (E154) K. Abe et al., Phys. Lett. B 405, 180 (1997).
93. C. Bourrely, F. Buccella, O. Pisanti, P. Santorelli, and J. Soffer, Prog. Theor. Phys. 99, 1017 (1998).
94. L. E. Gordon, M. Goshtasbpour, and G. P. Ramsey, Phys. Rev. D 58 , 094017 (1998); G. P. Ramsey, Prog. Part. Nucl. Phys. 39, 599 (1997).
95. E. Leader, A. V. Sidrov, and D. B. Stamenov, Phys. Lett. B 445, 232 (1998).
96. E. Leader, A. V. Sidrov, and D. B. Stamenov, Phys. Lett. B 462, 189 (1999).

97. Y. Goto, et al., Phys. Rev. D 62 , 034017 (2000).
98. D. de Florian, O. A. Sampayo and R. Sassot, Phys. Rev. D 57, 5803 (1998). D. de Florian and R. Sassot, Phys. Rev. D 62, 094025 (2000).
99. M. Fukugita, Y. Kuramashi, M. Okawa, and A. Ukawa, Phys. Rev. Lett. 75 , 2092 (1995).
100. S. J. Dong, J.-F. Lagae, and K-F. Liu, Phys. Rev. Lett. 75 , 2096 (1995).
101. M. Gockeler, et al., Phys. Rev. D 53 , 2317 (1996).
102. S. Guskin et al., Phys. Rev. D 59 , 114502 (1999).
103. I. I. Balitsky, V. M. Braun and A. V. Kolesnichenko, Phys. Lett. B 242 , 245 (1990); Phys. Lett. B 318 , 648 (1993).
104. X. Ji and P. Unrau, Phys. Lett. B 333 , 228 (1994);
105. (H1) S. Aid et al., Nucl. Phys. B 445 , 3 (1995); contributed paper to ICHEP97, Jerusalem (1997).
106. J. Respond, proceedings of workshop ‘Deep Inelastic Scattering and Related Phenomena,’ Rome 1996, Eds. G. D’Agostini and A. Nigro (World Scientific, Singapore, 1997) 439.
107. A. De Roeck et. al, hep-ph/9610315.
108. J. Feltesse, F. Kunne, E. Mirkes, Phys. Lett. B 388 , 832 (1996).
109. G. Rädcl, A. De Roeck, and M. Maul, hep-ph/9711373.
110. A. De Roeck et. al., Eur. Phys. J. C 6 , 121 (1999).
111. E. Mirkes and D. Zeppenfeld, Phys. Lett. B 380 , 205 (1996).
112. E. Mirkes and S. Willfahrt, hep-ph/9711434.
113. G. Rädcl and A. De Roeck, hep-ph/9909403.
114. M. Glück and W. Vogelsang, Z. Phys. C 55 , 353 (1992); Z. Phys. C 57 , 309 (1993); M. Glück, M. Stratmann, and W. Vogelsang, Phys. Lett. B 337 , 373 (1994).
115. M. Stratmann and W. Vogelsang, Z. Phys. C 74 , 461 (1997).
116. J. M. Butterworth, N. Goodman, M. Stratmann, W. Vogelsang,

Proceedings of the 1997 Workshop on Physics with Polarized Protons at HERA , Hamburg, Germany, Sept. 1997.

117. A. Bravar, D. von Harrach, and A. Kotzinian, Phys. Lett. B 421, 349 (1998).
118. M. Fontannaz, D. Schiff, B. Pire, Z. Phys. C 8, 349 (1981).
119. M. Glück, E. Reya, and W. Vogelsang, Nucl. Phys. B 351, 579 (1991); A. D. Watson, Z. Phys. C 12 , 123 (1982).
120. G. Baum et al, COMPASS. A Proposal for a Common Muon and Proton Apparatus for Structure and Spectroscopy/, CERN/SPSLC/96-14, SPSC/P,297 (1996), <http://wwwcompass.cern.ch/compass/proposal/welcome.html>.
121. I. Bojak and M. Stratmann, Nucl. Phys. B 540 , 345 (1999).
122. A. P. Contogouris, Z. Merebashvili, and G. Grispos, Phys. Lett. B 482, 1(2000).
123. G. Japaridze, W-D. Nowak and A. Tkabladze, Phys. Rev. D 62, 034022 (2000).
124. E. Berger and J. W. Qiu, Phys. Rev. D 44 , 2002 (1991).
125. S. Frixione and W. Vogelsang, Nucl. Phys. B 568 , 60 (2000).
126. Z. Dziembowski and J. Franklin. J. Phys. G17:213-220, 1991.
127. R. C. Hwa and M.S. Zahir, Phys. Rev. D23, 2539 (1981).
128. X. Que-bing, Phys. Rev. D26, 2261 (1982).
129. B.A. Campbell, J. Ellis and R,A. Flores, Phys. Left. B 225 (1989)419.
130. SMC, B. Adeva et al. Phys. Rev. D 70 , 012002 (2004) [arXiv:hep-ex/0402010].
131. D. Adams et al. ,SMS Collaboration: Phys. Lett B329 (1994)399.
132. A. V. Efremov and O. V. Teryaev. Czech. Hadron symp. 1988: 302.
133. STAR Collaboration (B. I. Abelev et al.). Oct 2007. 7pp [arXiv:hep-ex/0710.2048].
134. G. Altarelli and G.G. Ross, Phys. Lett. B212: 391, 1988.

135. B. Jäger, M. Stratmann and W. Vogelsang, Phys. Rev. D 70, 034010 (2004) [arXiv:hep-ph/0404057].
  136. B. Jäger, A. Schafer, M. Stratmann and W. Vogelsang, Phys. Rev. D 67, 054005 (2003) [arXiv:hep-ph/0211007].
  137. M. Glück, E. Reya, M. Stratmann and W. Vogelsang, Phys. Rev. D 63, 094005 (2001) [arXiv:hep-ph/0011215].
  138. S. Gupta, D. Indumathi, M.V.N. Murthy: Z. Phys. C42:493 (1989), Erratum-ibid. C44:356, 1989.
  139. D.B. Kaplan and A. Manohar, Nucl. Phys. B 310 (1988) 527.
  140. J. Ellis and M. Karliner, Phys. Lett. B 213 (1988) 73.
  141. L.A. Ahrens et al., Phys. Rev. D 35 ( 1987 ) 785.
  142. F.E. Close, Oak Ridge preprint (1989).
  143. S. Brodsky, J. Ellis and M. Karliner, Phys. Lett. B206, 309 (1988).
  144. T. P. Cheng and L. F. Li, Phys. Rev. Lett. 62, 1441 (1989).
  145. A. Airapetian et al. [HERMES Collaboration], Phys. Rev. D75: 012007, (2007).
  146. V. Y. Alexakhin et al. [COMPASS Collaboration], Phys. Lett. B647:8-17, (2007).
  147. H. Fritzsche, CERN-TH-2647, Mar 1979. 6pp.
  148. S. Gasiorowicz and J. L. Rosner, Am. J. Phys. 49: 954, 1981.
-